Computational Studies on Organo-catalyzed Selective Acylation of Carbohydrates

by

Gabriel Andrés Cintrón-Rosado

BS, Universidad de Puerto Rico, 2013

Submitted to the Graduate Faculty of the

Dietrich School of Arts & Sciences in partial fulfillment

of the requirements for the degree of

Master of Science

University of Pittsburgh

2018

UNIVERSITY OF PITTSBURGH

Dietrich School of Arts & Sciences

This thesis was presented

by

Gabriel Andrés Cintrón-Rosado

It was defended on

November 16th, 2017

and approved by

Tara Meyer, Professor, Department of Chemistry

Kazunori Koide, Associate Professor, Department of Chemistry

Thesis Director: Peng Liu, Assistant Professor, Department of Chemistry

Computational Studies on Organo-catalyzed Selective Acylation of Carbohydrates

Gabriel Andrés Cintrón-Rosado, M.S.

University of Pittsburgh, 2018

To explain the catalyst-dependent site-selective acylation of carbohydrates, we utilized density functional theory (DFT) calculations to model the corresponding transition states. In doing so it was discovered that the selectivity of the reactions depends on the presence or absence of a cation–*n* interaction between the cation in the acylated catalyst and an appropriate oxygen lone pair in the substrate. Overall, these studies allowed for the construction of a predictive model for site-selectivity, which is validated by various substrates.

TABLE OF CONTENTS

LIST OF TABLES

LIST OF FIGURES

INTRODUCTION: COMPUTATIONAL STUDIES OF ORGANO-CATALYZED ACYL TRANSFER REACTIONS

Non-enzymatic enantioselective acyl transfer reactions have been an active area of research for more than two decades. [1] Structurally diverse chiral catalysts based on amidines have been designed and synthesized for the purpose of functioning as catalysts that can perform kinetic resolutions of alcohols and related stereoselective transformations. In particular, chiral 4-dimethylamino-pyridine (DMAP) derivatives and bicyclic amidines have been demonstrated to be effective at catalyzing enantioselective acyl-transfer reactions to alcohols. [2]

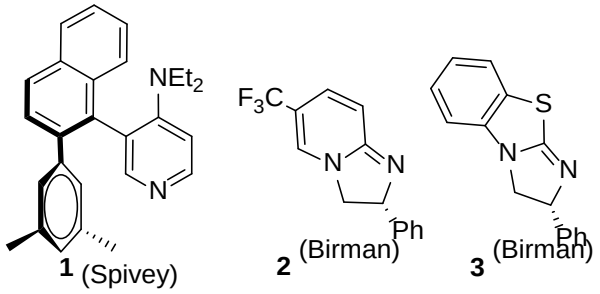

1 (Spivey) **2** (Birman) **3** (Birman)

Figure 1. Representative Structures of 4-DMAP derivatives and Amidine-Based Catalysts Used for the Kinetic Resolution of Alcohols

1.1 COMPUTATIONAL STUDIES OF CATALYTIC CYCLE FOR CHIRAL DMAP CATALYZED ACYL-TRANSFER REACTION

The Spivey and Zipse research groups collaborated in the design of chiral DMAP analog **1.**[3] This structure is shown to catalyze a kinetic resolution of 1-(1naphthyl)ethanol under the conditions reported on.

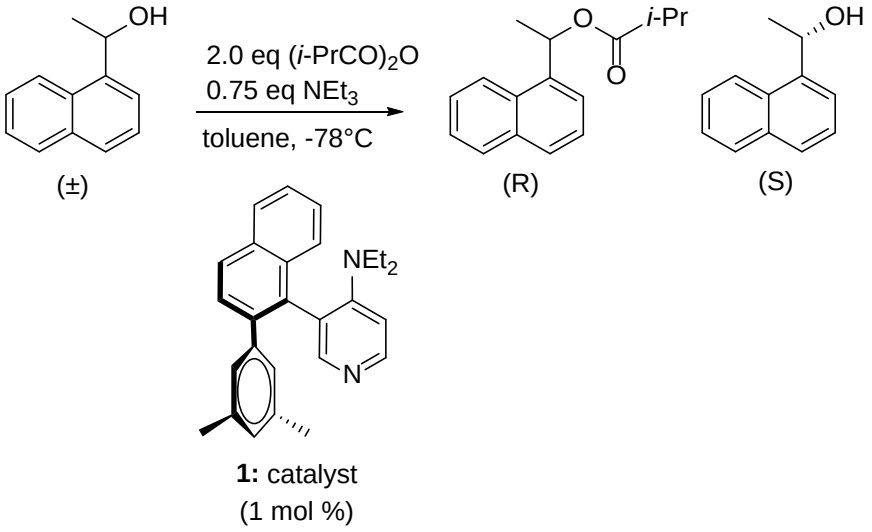

Figure 2 Chiral DMAP Catalyzed Kinetic Resolution of 1-(1naphthyl)ethanol

Catalyst **1** prefers to acylate the (R) enantiomer. Seeking to rationalize this phenomenon, Zipse and Spivey turned to computational modeling of transition states, where they employed density functional theory (DFT) to study the mechanism of this process. **Figure 3** shows calculated activation free energy barriers for the catalytic cycle of chiral DMAP analog **1**.

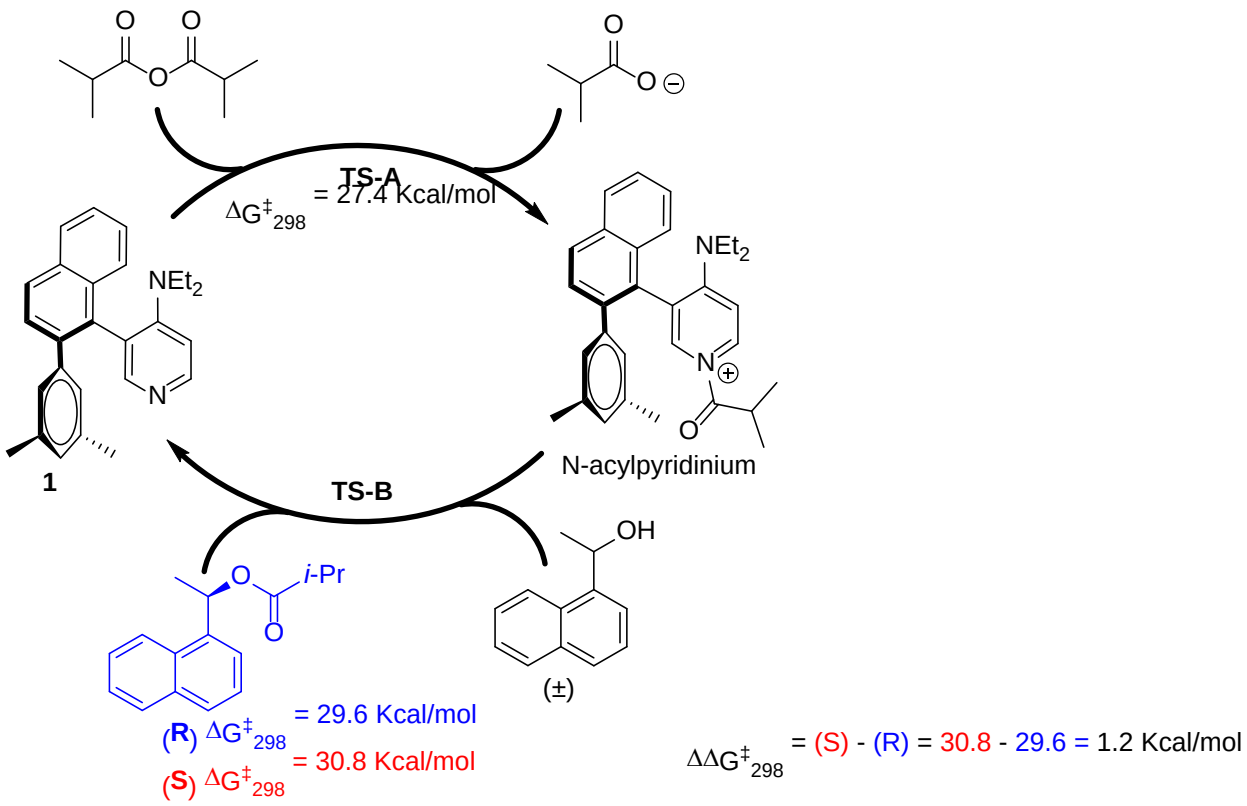

Figure 3 Relative Free Energies $\Delta G^{\ddagger}_{298}$ (in kcal mol^{-1}) for Stationary Points Located on the Potential Energy Surface at the B3LYP/6-311+G(d,p)//B3LYP/6- 31G(d) Level in the Gas Phase for the Acylation of Racemic 1-(1-naphthyl)ethanol Promoted by Chiral DMAP Derivative **1**

This catalytic cycle has two steps. **TS-A** is a fast step (lower barrier) where the catalyst is acylated to form a N-acylpyridinium intermediate. This N-acylpyridinium salt will then act and an electrophile in **TS-B** and transfer the acyl group to a specific alcohol enantiomer substrate. The formation of the ammonium intermediate (**TS-A**) has a lower calculated free energy ($\Delta G^{\ddagger}_{298}$ = 27.4 Kcal/mol) than alcohol's acylation by the catalyst (**TS-B**), (**(R)** $\Delta G^{\ddagger}_{298}$ = 29.6 Kcal/mol, and **(S)** $\Delta G^{\ddagger}_{298}$ = 30.8 Kcal/mol). **TS-B** is the rate-determining step for the catalytic cycle and the enantioselectivity determining step.

The free energy difference between the diastereoisomeric TSs of the rate-determining step ($\Delta\Delta G^{\ddagger}_{298}$ = 1.2 Kcal/mol) is the key value for predicting the which enantiomer reacts faster with the catalyst. In this case, the TS that leads to the **(R)** product (blue) has a predicted lower barrier, meaning it is favored over the **(S)** product. This prediction matched the experimentally observed selectivity.

1.2 COMPUTATIONAL STUDIES OF CF_3-PIP-CATALYZED KINETIC RESOLUTION OF BENZYL ALCOHOLS

The Vladimir B. Birman group designed CF_3-PIP **2**, a first-generation acyl transfer catalyst, which proved to be effective in the kinetic resolution of secondary benzylic alcohols. [4]

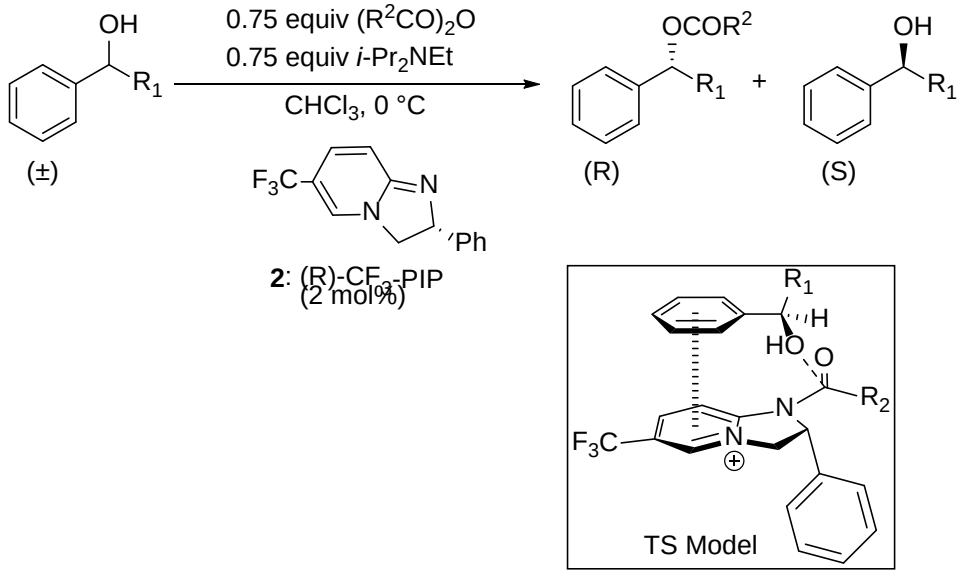

Figure 4 CF_3-PIP-Catalyzed Kinetic Resolution of Benzyl alcohols

Under the experimental conditions described by Birman, catalyst (R)-CF_3-PIP will selectively resolve a kinetic resolution of benzylic alcohols by selective acylation of the **(R)** enantiomer.

This kinetic resolution was computationally studied in a collaboration between Houk and Birman. Similar to the previous example, density functional theory (DFT) was utilized to calculate the hypothesized TS Model and explain the enantioselectivity in the observed in the kinetic resolution.

To locate the lowest energy transition state geometry, a transition state conformational search was performed on a model system. This led to the identification of the most stable TS conformers **TS-1**, **TS-2**, **TS-3**, and **TS-4**).

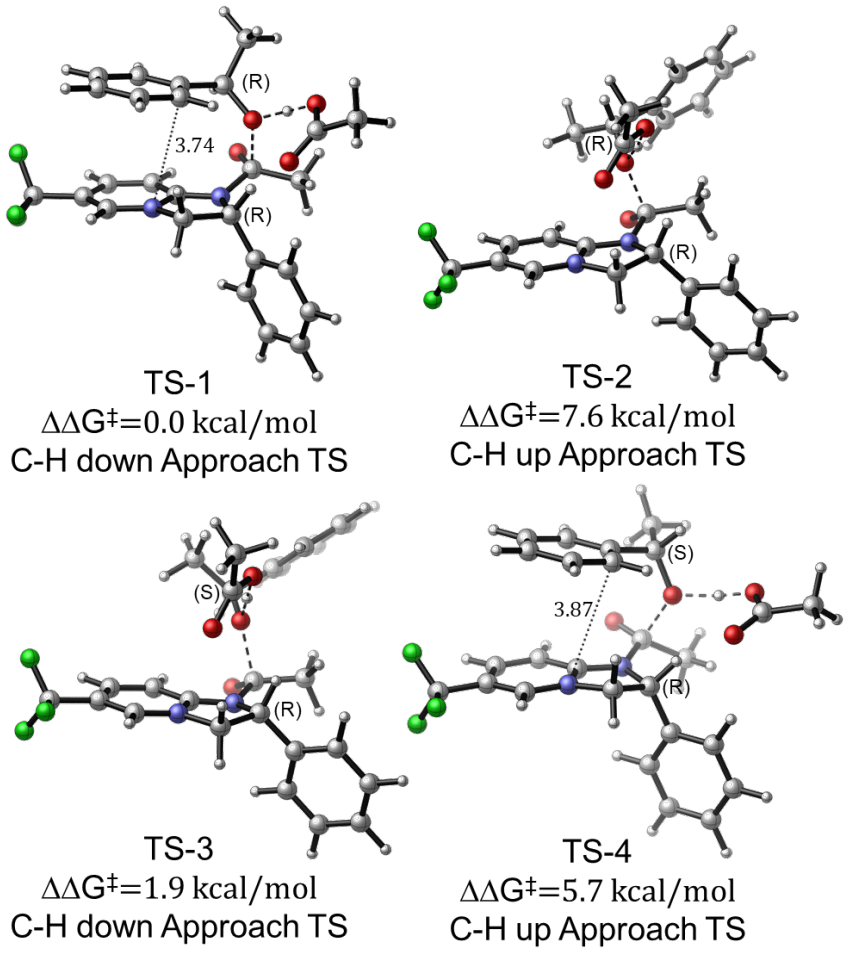

Figure 5 Transition states for reactions of (R)- and (S)-phenylethanol with (R)-CF_3-PIP

In these TS conformers the **(R)**, **(S)** – phenylethanol substrate approaches the catalyst (R)-CF_3-PIP from two orientations. Conformer **TS-1** has the lowest calculated free energy difference between the TS conformers shown. The **TS-1** structure positions the aromatic part of the substrate on top of the catalyst. The authors speculate this will lead to a cation-π interaction which stabilizes **TS-1**.

To further understand the nature of this cation-π interaction, Houk and Birman calculated the interaction energy between the CF_3-PIP and a molecule of benzene at different distances.

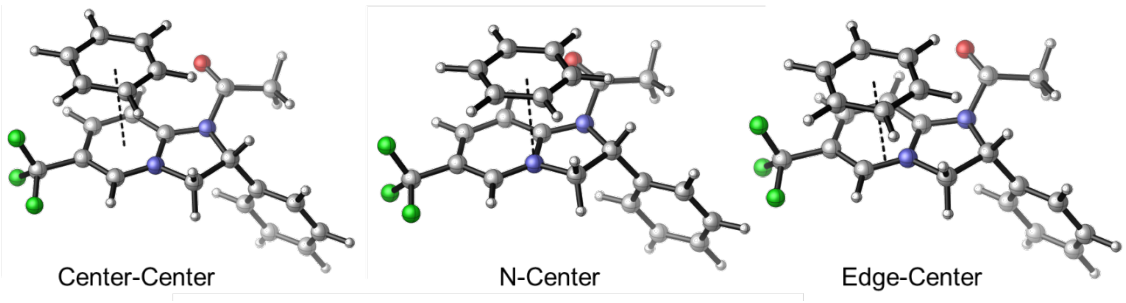

Figure 6 Interaction modes of benzene and N-acylpyridinium-CF_3-PIP [4h]

The intermolecular distances are the distance between the centers of benzene and pyridinium ring (center-center), between the pyridinium nitrogen and the center of benzene (N-center), and between the midpoint of the N-C bond and the center of benzene (edge-center). The interaction energy between benzene and N-acylpyridinium-CF_3-PIP is highest at distances between 3.5 and 4 Å.

This distance range matches what is observed in **TS-1** conformer, in which the distance between the aromatic rings is 3.74 Å. In summary, this study supported the TS Model in which the catalyst's pyridinium ring interacts with the substrate's aromatic system by way of cation-π interactions and rationalized the observed enantioselectivity in the kinetic resolution.

1.3 COMPUTATIONAL STUDIES OF (R)-BTM-CATALYZED KINETIC RESOLUTION OF 2-HYDROXYALKANOATES

In another example of computationally studied catalyst-controlled kinetic resolutions, Shiina et al. discovered that a racemic mixture of 2-hydroxyalkanoates substrates would also undergo a kinetic resolution when using **3** (R)-benzotetramisole (**(R)-BTM**). [5]

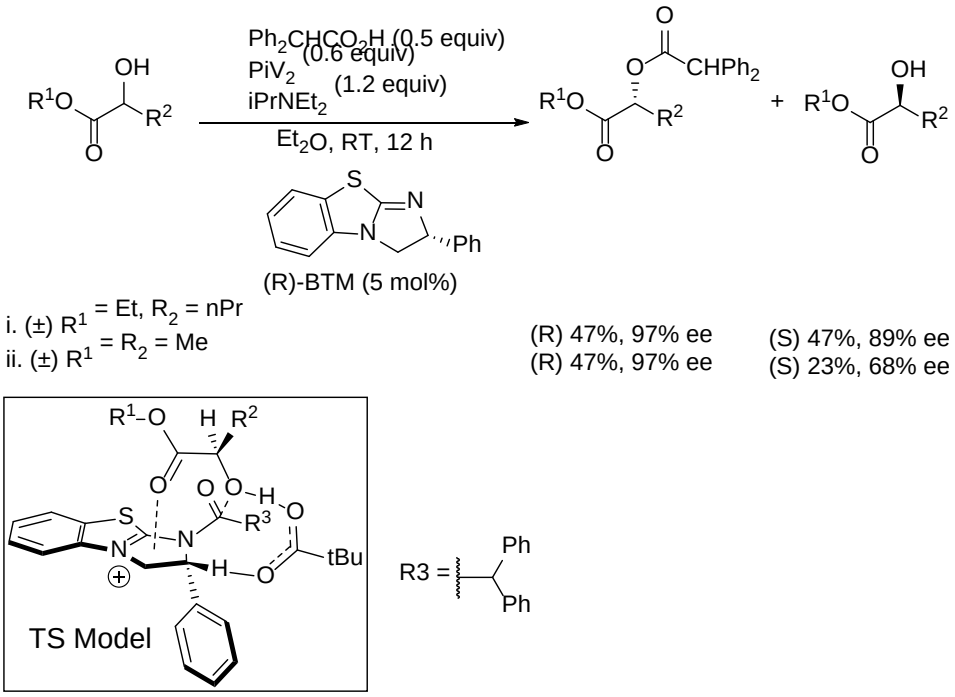

Figure 7 (R)-BTM-Catalyzed Kinetic resolution of racemic ethyl 2-hydroxypentanoate and methyl lactate

Similar to the previous example by Birman, Shiina utilized a transition state conformational search to the locate the most stable TS conformers (**TS-R, TS-S-a, TS-S-b**).

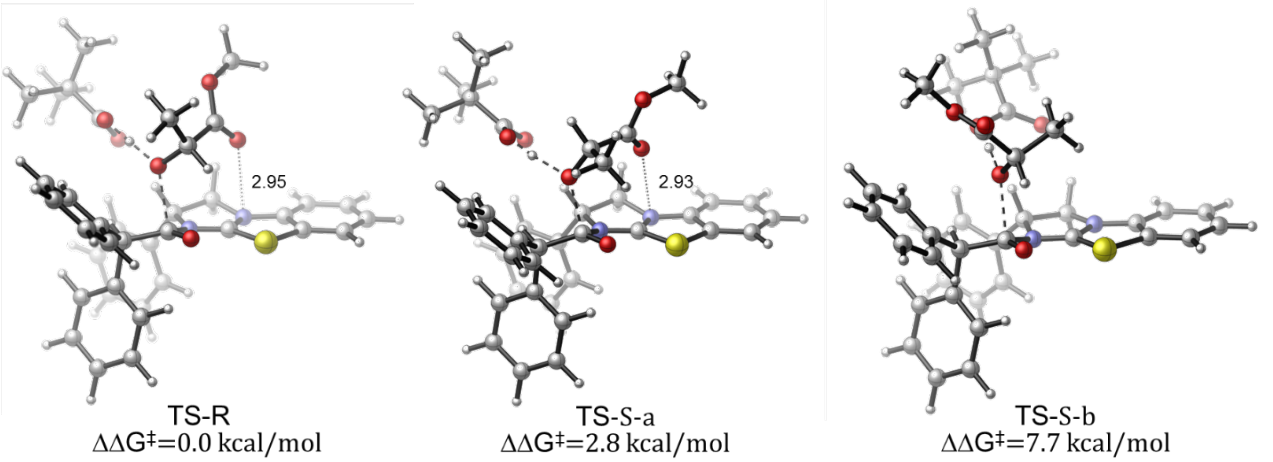

Figure 8 Transition states for reactions of (R)- and (S)- ethyl 2-hydroxypentanoate with (R)-BTM

In this case, conformational analysis identified the two most stable TS conformations (**TS-R** $\Delta\Delta G^{\ddagger}_{298}$ = 0.0 Kcal/mol, **TS-S-a** $\Delta\Delta G^{\ddagger}_{298}$ = 2.8 Kcal/mol). Based on the DFT calculations, Shiina proposes that these conformations are stabilized by an attractive interaction of between the oxygen in the ester carbonyl group and the positive charge on the face of the imidazolium salt. Rotating this oxygen atom away from the catalyst (**TS-S-b**) destabilizes the TS conformation as evidenced by the higher calculated free energy difference for TS-S-b, $\Delta\Delta G^{\ddagger}_{298}$ = 7.7 Kcal/mol)

1.4 THESIS OBJECTIVES

In the reported examples, transition state computational models have been shown to be great tools for explaining the experimental selectivity of enantioselective acyl transfer reactions. Computational models provide the ability to segregate and quantify the interactions in the

selectivity-determining transition state that favor the formation of one enantiomeric product versus another.

I would like to extent a similar approach and study some reported examples reported by Tang et al. in which carbohydrate substrates are acylated using chiral organocatalysts. [6] [7]

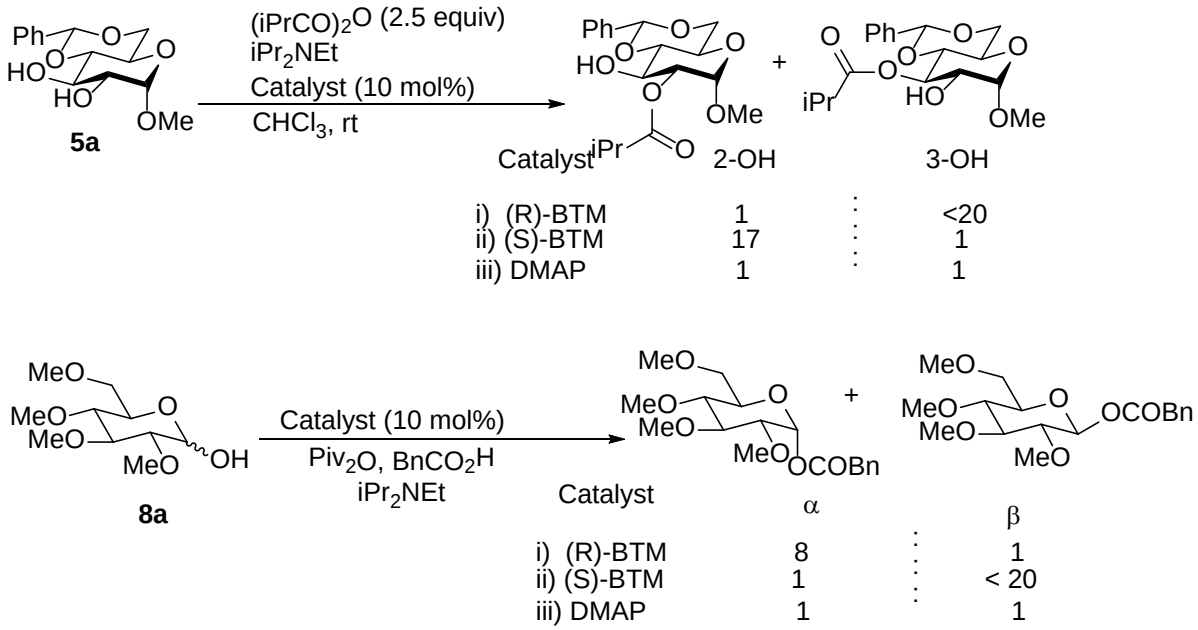

Figure 9 Organo-catalyzed Selective Acylation of Carbohydrates reported by Tang et al.

These reactions make use chiral amidine-based organocatalysts but, experience different interaction modes between the catalyst and substrate.

By studying the catalyst substrate interactions involved in each possible transition state conformation the observed selectivity can be rationalized. The goal is to compile a reliable set of rules that could be used to predict selectivity on a variety of substrates. These insights will provide a guide for the future development of experimental systems.

2.0 COMPUTATIONAL STUDIES ON THE SITE-SELECTIVE ACYLATION OF CARBOHYDRATES

2.1 EXPERIMENTAL RESULTS FOR THE SITE-SELECTIVE ACYLATION OF *TRANS*-1,2-DIOLS IN CARBOHYDRATES

Recently, Tang's research group has reported an example of a organocatalyst-controlled acylation of lactols.[7] The reported methodology utilizes amidine based chiral organocatalysts (R)-BTM, its enantiomer (S)-BTM together with 4-dimethylaminopyridine (DMAP) for site-selective acylation of α-glucose derivatives **5a** and **5b** with a free 2-O/3-O diol using isobutyric anhydride as the acylation reagent.

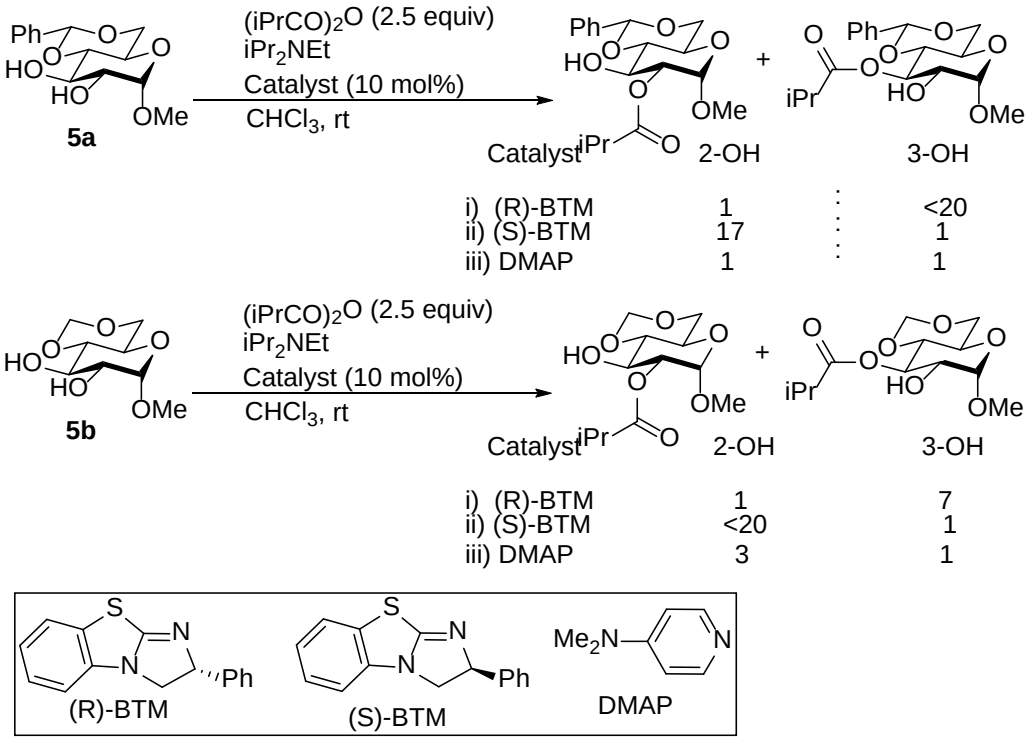

Figure 10 Site-selective acylation of 2-O/3-O Diols in Glucosides **5a** and **5b**

The 3-OH in α-glucoside **5a** can be selectively acylated to using (R)-BTM catalyst, while the 2-OH was selectively acylated using (S)-BTM. In contrast, a 1:1 ratio of 2-OH: 3-OH selectivity was observed when using DMAP (achiral) as the catalyst.

When the protecting group was changed from benzylidene group in **5a** to methylene group in **5b**, the 2-OH is intrinsically favored for acylation, (2-OH/3-OH = 3:1) using DMAP as the catalyst. While (R)-BTM can override the intrinsic selectivity to yield afford the 3-O product as the major isomer, (S)-BTM catalyst enhanced the intrinsic the 2-O selectivity to a ratio of <20:1.

The dramatically different selectivity between the selected glucosides suggest that these reactions are under catalyst control.

2.2 PROPOSED CATALYTIC CYCLE SITE-SELECTIVE ACYLATION OF 2-OH/3-OH DIOLS CATALYZED BY (R)-BTM

We postulated that the mechanism for the site-selective acylation of 2-OH/3-OH diols in glucosides **5a** and **5b** would follow a similar catalytic the acylation pathway to the one reported by Spivey and Zipse et al. [3]

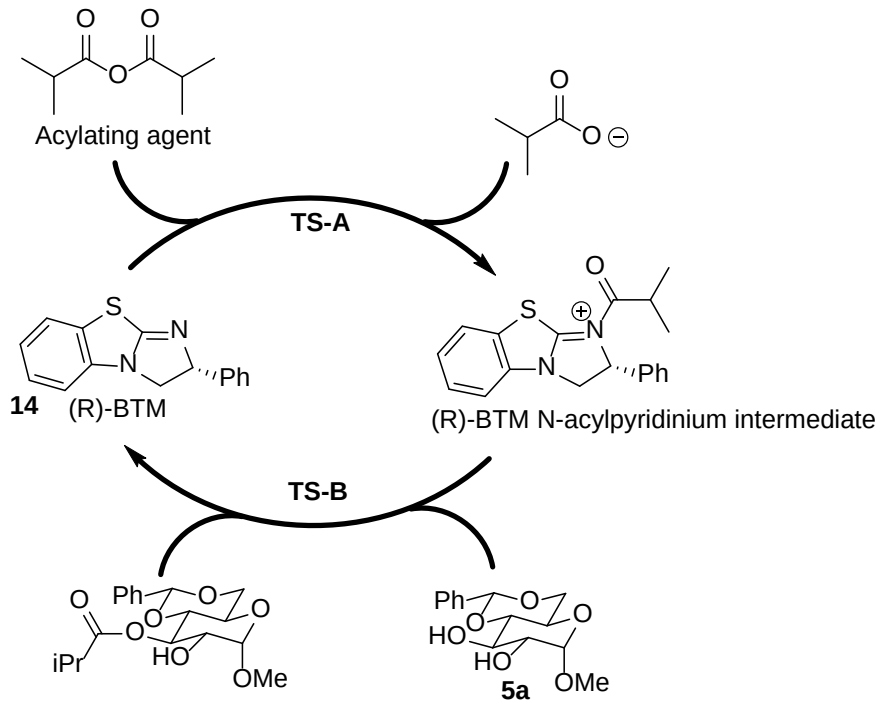

Figure 11 Postulated Mechanism for them Site-selective acylation of 2-OH/3-OH Diols catalyzed by (R)-BTM

The catalytic cycle has two steps. **TS-A** is fast step (lower barrier) where the catalyst is acylated to form an (R)-BTM N-acylpyridinium intermediate. **TS-B,** the site-selective determining step, describes the acylation of the alcohol substrate by the N-acylpyridinium intermediate.

As described by Zipse, nucleophilic attack to the carbonyl and the alcohol deprotonation by the acetate ion pair happens in a concerted step. Our goal is to study what catalyst substrate interactions are possible in different transition state conformations. Understanding the underlined principles that govern the geometry of TS-B will allow for the proposal of a predictive model for the site-selectivity of glucosides **5a** and **5b.**

2.3 CONFORMATIONAL ANALYSIS FOR SITE-SELECTIVE ACYLATION TRANSITION STATES

To study the site-selective determining step, a careful conformational study of transition state structure geometry was performed by systematically examining geometries around two dihedral angles.

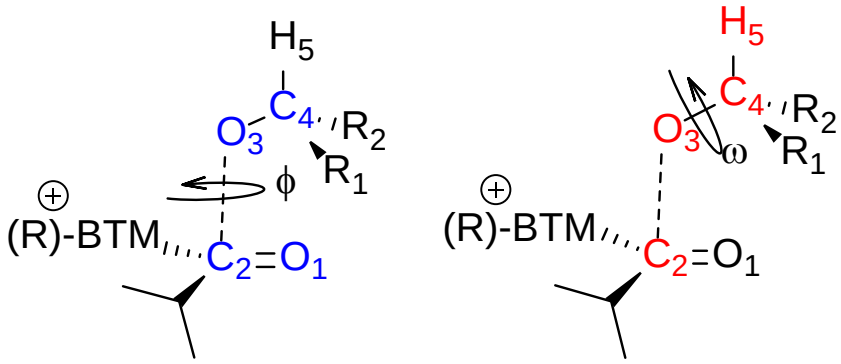

Figure 12 Dihedral Angles Rotated in Conformational Study of Acylation Transition States

Dihedral angle ϕ is centered around forming C_2-O_3 bond. Fixing in space the O_1=C_2 bond allows for the rotation of the top O_3-C_4 bond.

The other dihedral angle ω is centered around the substrate O_3-C_4 σ bond. By fixing in space the forming C_2-O_3 we can rotate the C_4-H_5. By varying these two angles we can change the direction and side of the substrate that approaches the catalyst.

The substrate sugar has two different sides that can approach catalyst. One approach points the C−H bond on the carbon that is being acylated toward the carbonyl O ("**C−H down TS**"), or the C− H bond can be pointed away from the carbonyl O ("**C−H up TS**").

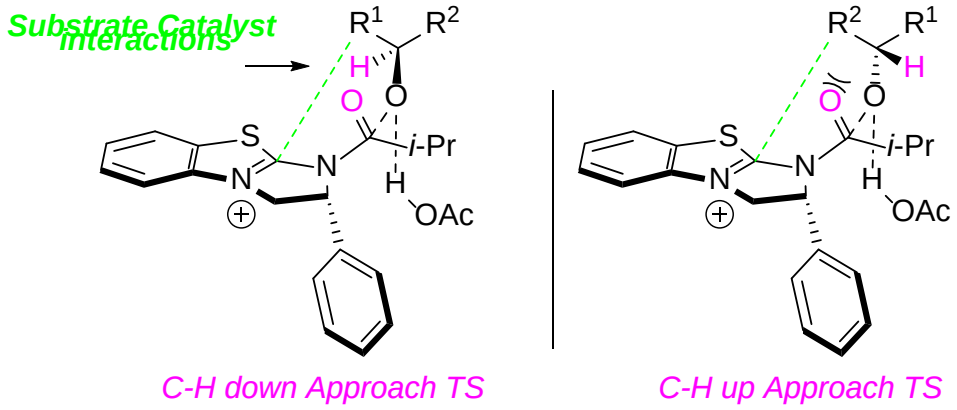

Figure 13 Two Orientations the Substrate Adopts when Approaching the BTM N-acylpyridinium intermediate

The two different approaches position different O-containing groups on the substrate to interact with the positively charged acylated catalyst. We suspect steric clash between the R group and the carbonyl oxygen will disfavor the "C-H up TS".

2.4 COMPUTATIONAL DETAILS

All DFT calculations reported were performed with Gaussian 09.[8] The transition state geometries were optimized using the M06-2X[9] density functional and the 6-31G(d) basis set in the gas phase. The "ultrafine" integration grid in Gaussian was used. Single-point energies were calculated using M06-2X with the 6-311++G(d,p) basis set and include solvation energy corrections calculated using the SMD[10] model. Chloroform was used as the solvent in the solvation energy calculations. The Gibbs free energies reported include zero-point vibrational energies and thermal corrections computed at 298K. The entropic contributions to the Gibbs free energies were calculated from partition functions using Cramer and Truhlar's quasiharmonic approximation,[11,12] which raises vibrational frequencies lower than 100 cm^{-1} to 100 cm^{-1} as a way to correct the harmonic oscillator model for low-frequency vibrational modes.

2.5 CONFORMATIONAL RESULTS FOR (R)-BTM-CATALYZED ACYLATION OF A-O-GLUCOSIDE 5A

The "C-H up", "C-H down" TS conformers for the acylation of **5a** with (R)-BTM are summarized in **Figure 13**. Experimentally this reaction favors 3-OH acylation with a 3-OH/2-OH ratio of 20:1.

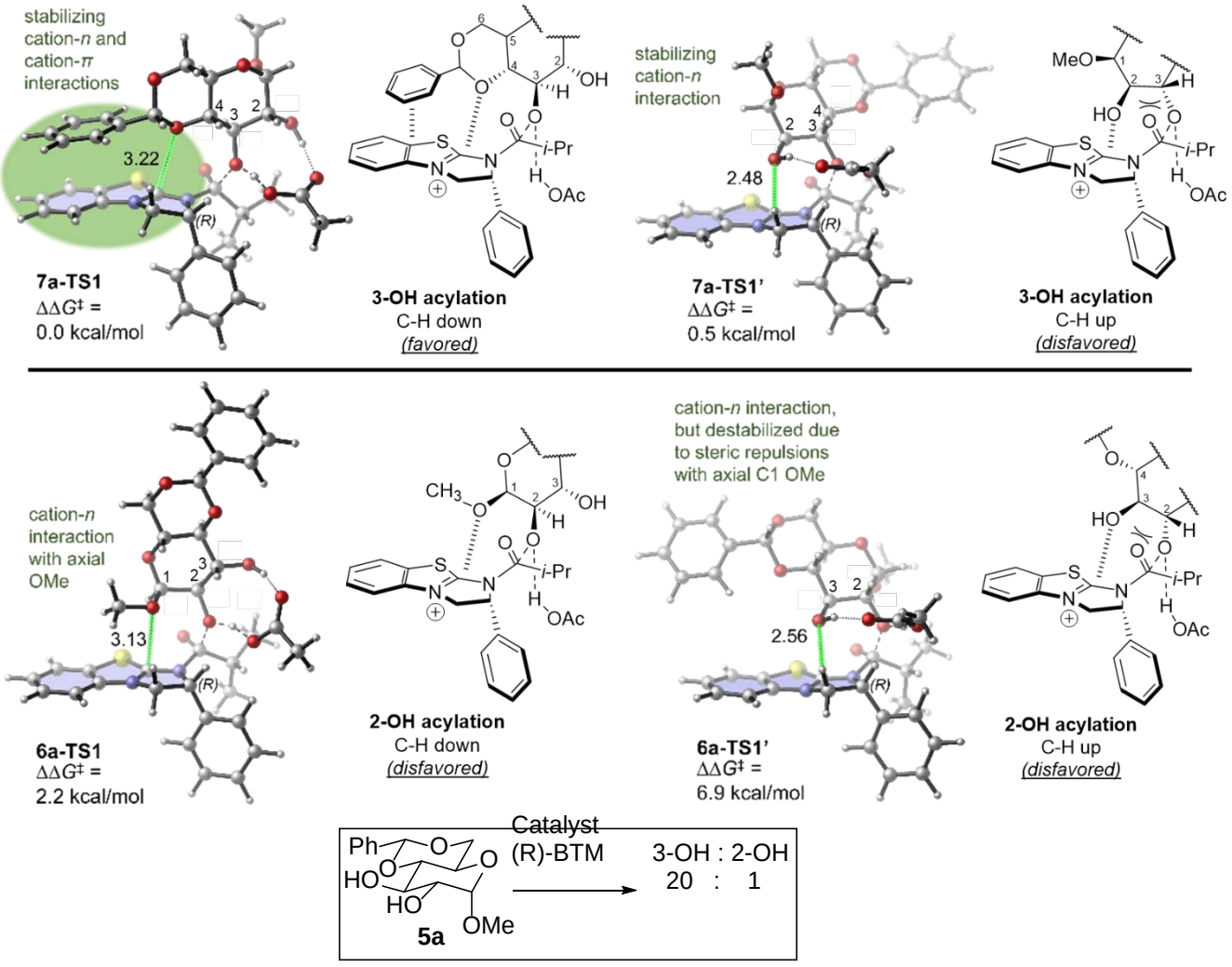

Figure 14 Transition state conformers of (*R*)-BTM-catalyzed acylation of α-O-glucoside **5a**.

The computed free energy difference ($\Delta\Delta G^{\ddagger}$), which is shown for each TS conformer, indicates that conformer **7a-TS1** ($\Delta\Delta G^{\ddagger}$= 0.0 Kcal/mol) is the computationally predicted product**.** **7a-TS1** is the "C-H down" TS for the 3-OH acylation which matches the experimentally observed selectivity.

In this conformation, the benzylidene protecting group is located above the BTM surface. We suspect this conformation is stabilized by a cation-π interaction between the aromatic group and the (R)-BTM N-acylpyridinium intermediate. In addition to this, the 4-O is also in proximity to the BTM positive surface and may participate in a cation-n interaction.

This **cation-n** interaction would be a charge-diploe type electrostatic interaction between an oxygen lone pair and the positively charged catalyst.

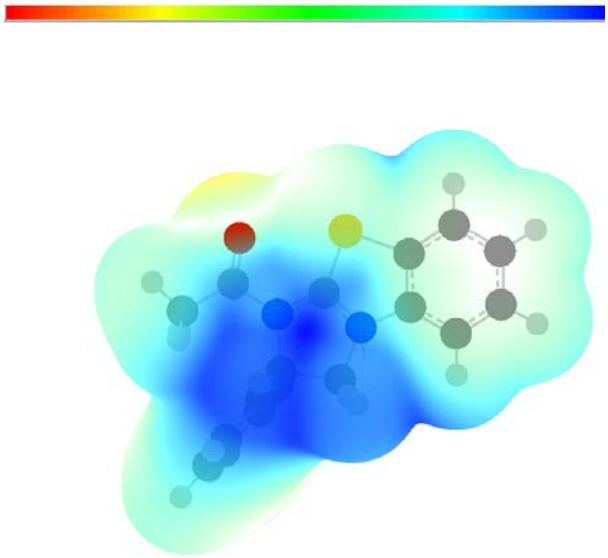

Figure 15 Electrostatic Potential Surface Map of the acylated catalyst

An Electrostatic Potential Surface (EPS) of the N-acylpyridinium intermediate is shown above. The blue coloring denotes positive potential, and red, negative potential. The N-acylpyridinium intermediate is cationic and is charged +1. The dark blue area above the catalyst amidine carbon contains the most positive region. If oxygen atoms pointing lone pairs towards this dark blue region are participating a cation-n interaction, examining how the strength of this interaction varies with different conformations may explain the observed selectivity.

The "C-H down" conformer for the 2-OH acylation, **6a-TS1** is computed 2.2 kcal/mol higher in energy. This conformation also features a cation-n interaction with the 1-OR axial group. We speculate axial 1-OR cation-n interaction is weaker because the oxygen lone pair pointed away from the catalyst.

The "C-H up" TS conformers for the 2-OH and 3-OH acylation were also computed (**7a-TS',6a-TS'**). The calculated free energy difference ($\Delta\Delta G^{\ddagger}$) for both was higher with an energy difference of $\Delta\Delta G^{\ddagger}$= 0.5 Kcal/mol $\Delta\Delta G^{\ddagger}$= 2.2 Kcal/mol, respectively, than the corresponding "C-H down" TS conformer. This confirms "C-H up" TS conformers are disfavored because steric repulsion between the R group and the carbonyl oxygen.

2.6 CONFORMATIONAL ANALYSIS RESULTS FOR (R)-BTM-CATALYZED ACYLATION OF A-O-GLUCOSIDE 5B

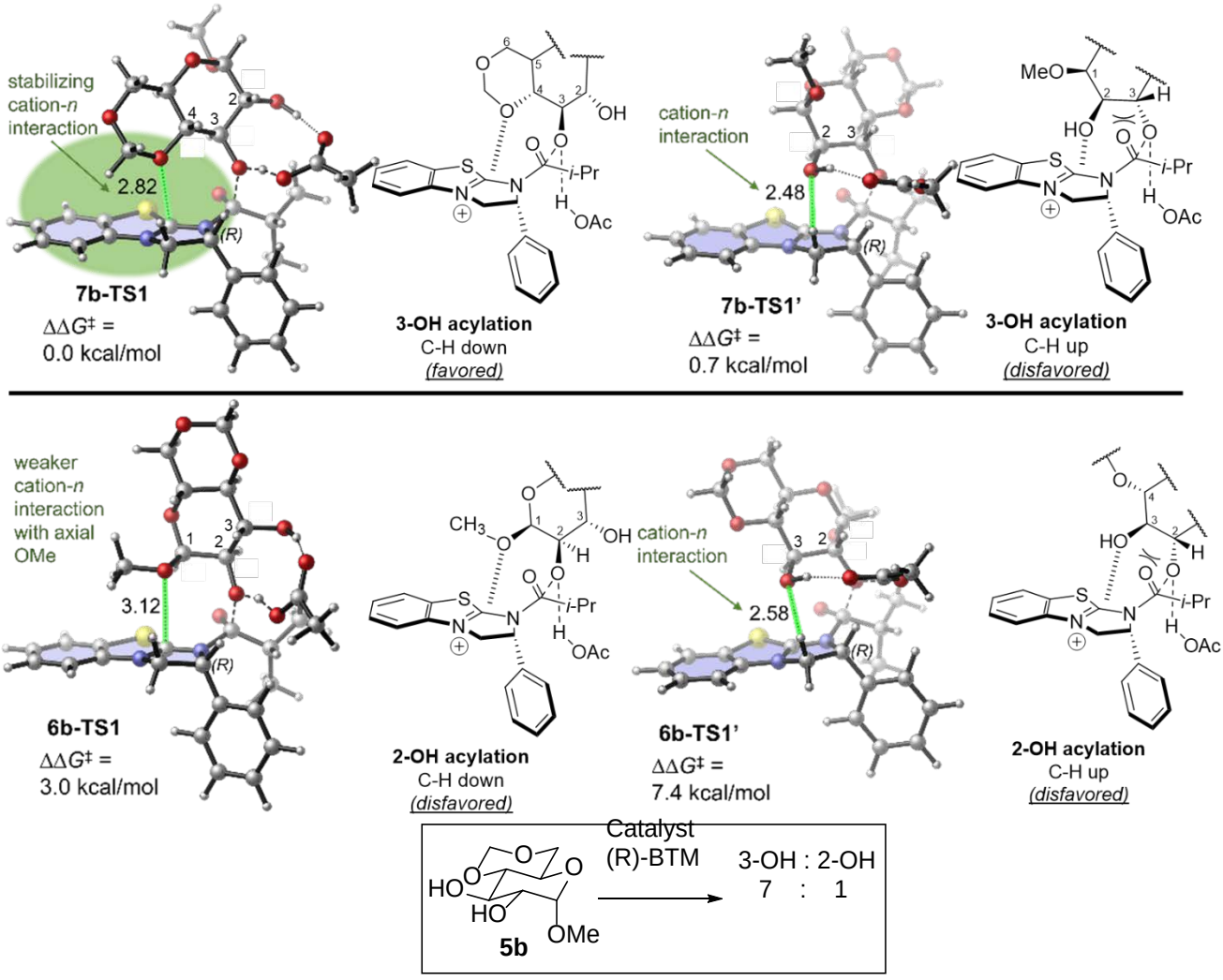

Figure 16 Transition state conformers of (*R*)-BTM-catalyzed acylation of α-O-glucoside **5b**.

When using (R)-BTM substrate **5b** will also display 3-OH selectivity. **7b-TS1** is the lowest energy TS conformer ($\Delta\Delta G^{‡}$= 0.0 Kcal/mol) which correctly matches the observed 3-OH selectivity. For **5a,** the 3-OH "C-H down" TS conformers was stabilized by a combination of cation-π and cation-

n interactions. Although **5b** lacks the benzylidene protecting group the 3-OH "C-H down" TS conformer is still lowest energy structure. This is because the 4-OR group is participating in a much stronger cation-n interaction evidenced by the distance (2.82 Å).

The 2-OH acylation "C-H down" TS conformer (**6b-TS1,** $\Delta\Delta G^{\ddagger}$= 3.0 Kcal/mol) has a much weaker cation-*n* interaction because the axial OMe group on 1-OR is not perfectly oriented towards the positively charged aromatic system in the acylated catalyst. The corresponding O−C distance between the O lone pair and the catalyst in **6b-TS1** is significantly longer (3.12 Å).

2.7 CONFORMATIONAL ANALYSIS RESULTS FOR (S)-BTM-CATALYZED ACYLATION OF A-O-GLUCOSIDE 5A

When using (S)-BTM as the acyl transfer catalyst on substrate **5a** the experimental selectivity now favors 2-OH acylation. The "C-H up" and "C-H down" TS conformers for the (S)-BTM reaction of **5a** are summarized below.

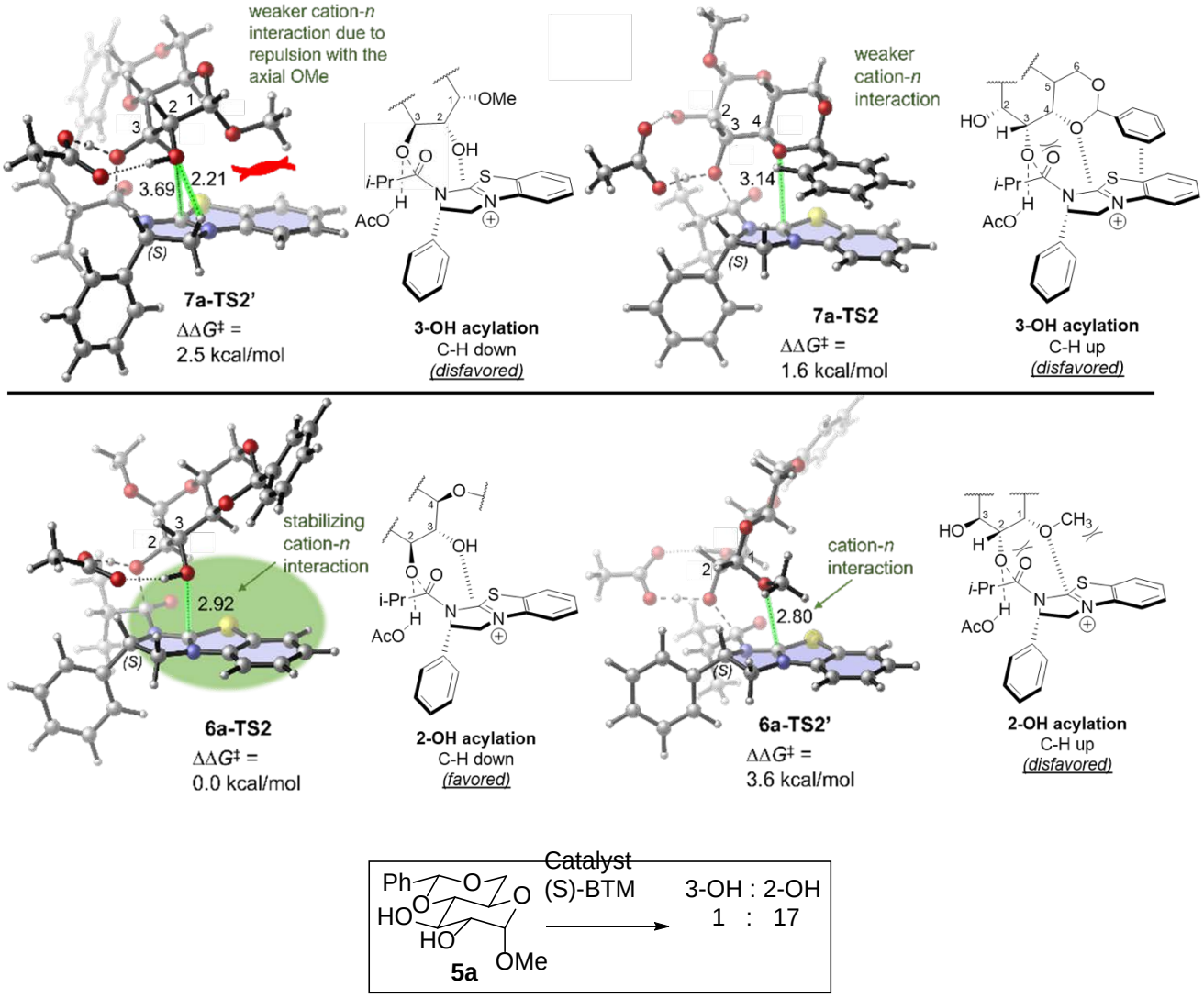

Figure 17 Transition state isomers of (*S*)-BTM-catalyzed acylation of α-O-glucoside **5a**.

The lowest energy TS conformer **6a-TS2** ($\Delta\Delta G^{\ddagger}$= 0.0 Kcal/mol) matches experimental observed selectivity in which the 2-OH acylation is favored 17:1. We suspect a cation-n interaction between the 3-O and the catalyst is stabilizing this TS conformer.

The 3-OH acylation "C-H down" conformer (**7a-TS2')** has the 2-O interacting with the catalyst but is disfavored, with a calculated energy 2.6 Kcal/mol higher, because the axial 1-OR group is causing steric repulsion against the catalyst.

2.8 CONFORMATIONAL ANALYSIS RESULTS FOR (S)-BTM-CATALYZED ACYLATION OF A-O-GLUCOSIDE 5B

The lowest energy TS conformer **6b-TS2** ($\Delta\Delta G^{\ddagger}$= 0.0 Kcal/mol) matches the experimental observed selectivity in which the 2-OH product is favored 20:1.

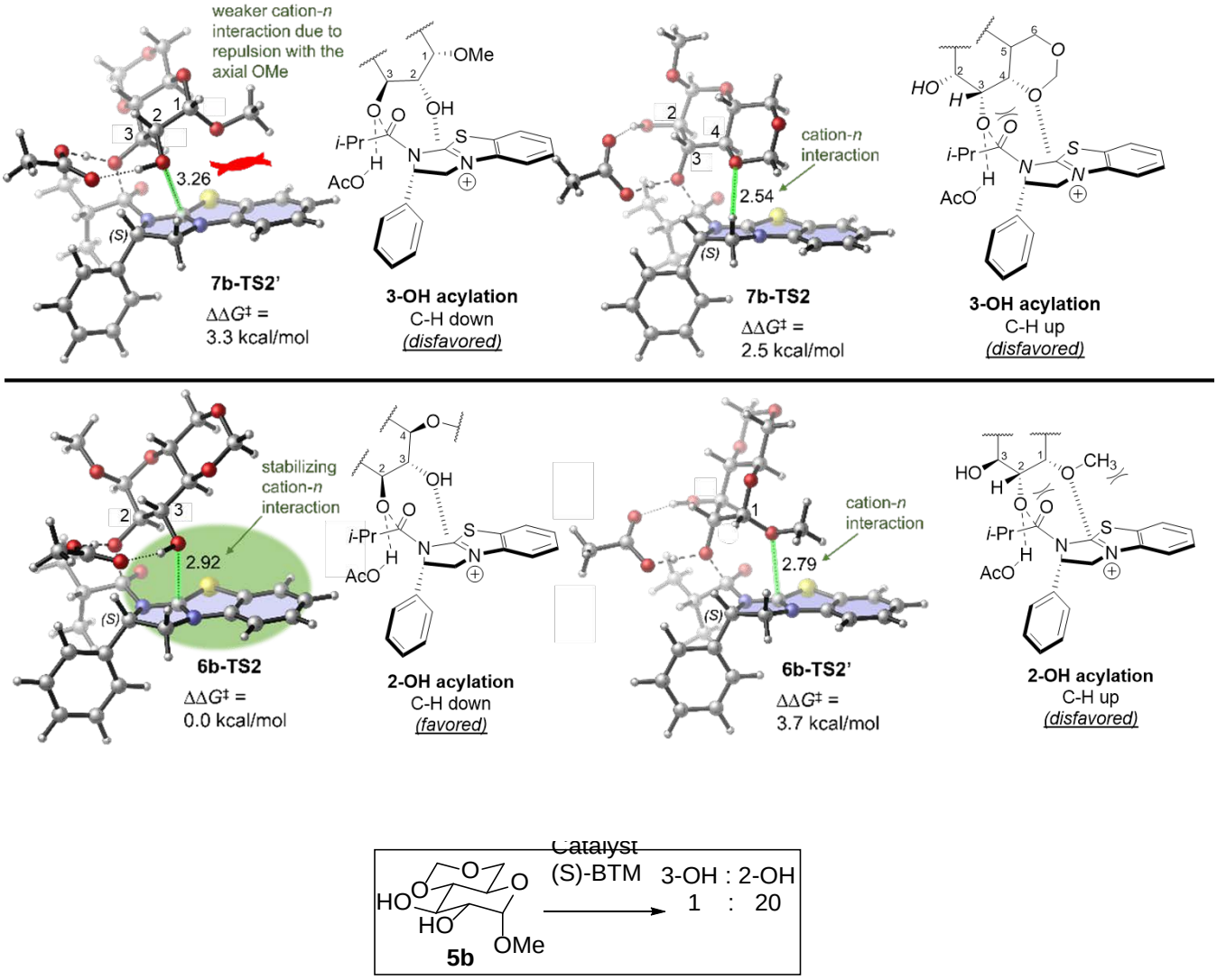

Figure 18 Transition state isomers of (*S*)-BTM catalyzed acylation of α-O-glucoside **5b**

Same as the previous case, the favored 2-OH acylation TS conformer (**6b-TS2**) is stabilized by a cation-n interaction between the 3-OR group and the acylated catalyst. The 3-OH acylation "C-H down" conformer (**7b-TS2')** has the 2-O interacting with the catalyst but is disfavored, with an energy of 3.3 kcal/mol, because the axial 1-OR group is causing steric repulsion against the catalyst.

2.9 CONFORMATIONAL ANALYSIS RESULTS DISCUSSION

The "C−H up" conformation leads to more significant steric repulsions between the acylated catalyst and the adjacent carbons on the substrate. Indeed, most of the lowest energy TS conformers calculated have the "C−H down" conformation to minimize the steric repulsions between the catalyst and the substrate. The only two exceptions are the (*S*)-BTM-catalyzed 3-OH acylation TS of α-O-glucosides **5a** and **5b**, in which the "C−H up" conformers (**7a-TS2** and **7b-TS2**) are 0.9 and 0.8 kcal/mol lower than in energy than the corresponding "C−H down" conformers (**7a-TS2'** and **7b-TS2'**, see **Figures 20 and 21**). Here the "C−H down" conformers **7a-TS2'** and **7b-TS2'** are destabilized due to the unfavorable steric repulsions between the axial OMe group and the catalyst. It should be noted that although **7a-TS2** is stabilized by a cation-π interaction with the benzylidene protecting group on the substrate, it is still less stable than **6a-TS2**, due to the unfavorable steric interactions in this "C−H up" conformation.

Since the nature of the cation-*n* interactions is most likely a charge-diploe type electrostatic interaction,[15] its strength is expected to be dependent upon the distance of the "**anchor**" O atom

and the cationic catalyst. In nearly all favored transition states with strong cation-*n* interactions (*e.g.*, **7b-TS1**, **6a-TS2**, **6b-TS2**), the distance between the "anchor" O atom and the amidine carbon in the catalyst is shorter than 3 Å. The only exception is **7a-TS1**, in which the O−C distance is 3.22 Å. This longer distance is necessary to achieve the favorable cation-π interaction with the benzylidene protecting group. In contrast, the corresponding O−C distance with the axial OMe group in **6a-TS1** and **6b-TS1** and with the 2-OH in **7a-TS2'** and **7b-TS2'** that is blocked by the adjacent axial OMe are all significantly longer than 3 Å, indicating significantly diminished cation-*n* interactions in these disfavored TSs.

The most favorable conformers of the acylation transition states revealed a fundamentally different origin of stereochemical control from that in the previous experimental systems, which is dominated by the cation-π interaction with aromatic substituents on the substrate.[14,15] Instead, the transition states (TSs) for the acylation of **5a** and **5b** feature a stabilizing cation-n interaction between the positively charged acylated catalyst and a lone pair on an OR or OH group of the substrate.

Taken together, the computational analysis indicated the cation-n interaction is sensitive to the stereochemical environment around the O lone pair. Although there are many TS conformers in each acylation pathway, the most favorable acylation TS always adapts the "C−H down" conformation to avoid substrate-catalyst steric repulsions and involves a stabilizing cation-*n* interaction as evidenced by a short distance between the "anchor" oxygen atom and the cationic catalyst. Depending on the stereochemistry around the O lone pair, cation-n interactions in the "C-H down" conformation are either favored or disfavored. A favorable interaction is only possible with equatorial OH and OR groups that are not blocked by an adjacent axial substituent.

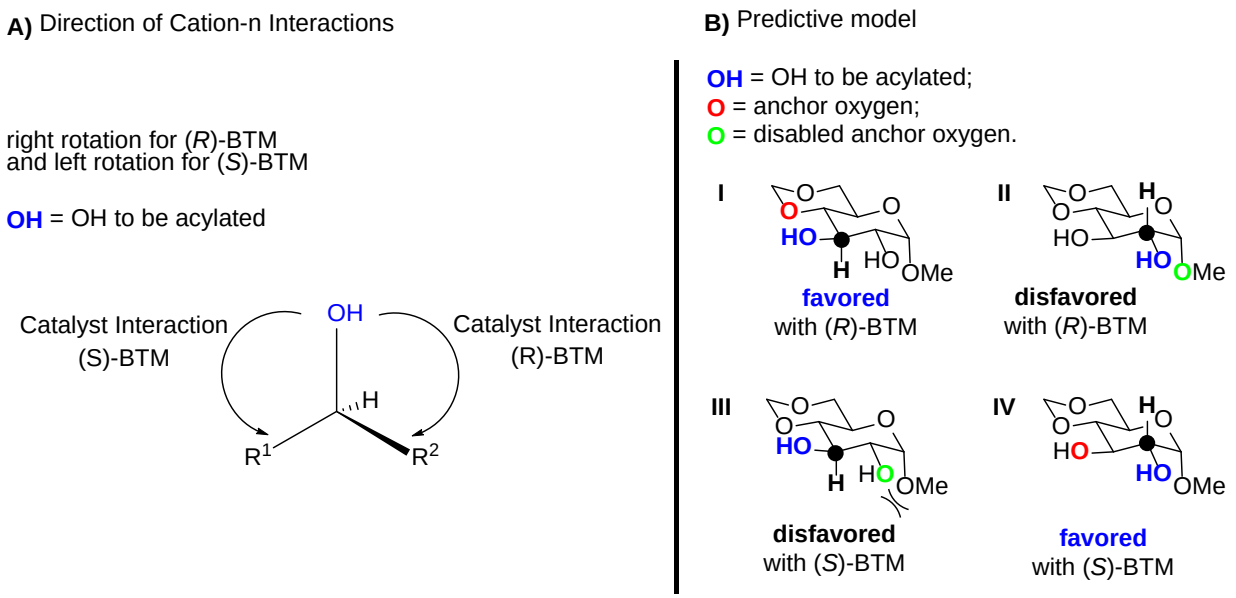

Figure 19 Predictive model for site-selectivity base on cation-n Interactions

In the case of (R)-BTM-catalyzed acylation (e.g. I and II, **Figure 19B**) 3-OH acylation is favored because the anchor 4-OR group on the substrate is equatorial and can form a strong cation-n interaction (defined as "anchor" O I). In case of substrates that have a benzylidene-protecting group (**5a**), the favorable cation-n interaction is augmented by a cation-π interaction that significantly stabilizes the 3-OH acylation TS. In the 2-OH acylation, the cation-*n* interaction is much weaker because the axial 1-OMe group is not perfectly oriented towards the positively charged aromatic system in the acylated catalyst ("disabled anchor" O in II).

In the reactions with the (*S*)-BTM catalyst (e.g. III and IV, **Figure 19B**), the site-selectivity is reversed to favor 2-OH acylation, because both are stabilized by a strong 3-O cation-*n* interaction ("anchor" O in IV). The cation-n interaction with 2-O is disfavored due to steric repulsions with the adjacent axial α-OMe group (disabled anchor O in III).

2.10 EXPERIMENTAL VALIDATION OF PREDICTIVE MODEL

Our predictive model based on cation-n interactions can be extended to analyze other monosaccharides.

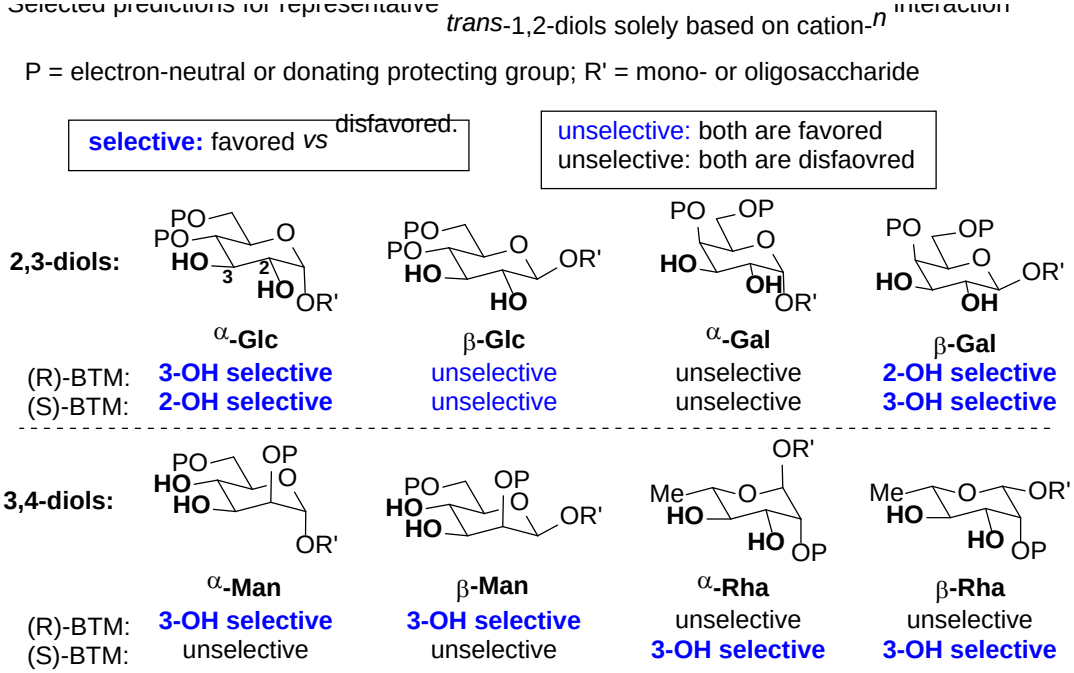

Figure 20 Predicted Site-Selectivity for Representative Carbohydrates

Based on the model above, we systematically analyzed the site-selectivity for the acylation of equatorial OHs in common carbohydrate building blocks, solely based on cation-n interactions. We have confirmed the selectivity for both α- and β-glucosides with a free 2-O /3-O diol.

No selectivity is expected for α-galactosides with a free 2-O /3-O diol, because the two OHs in α-galactosides are both disfavored using either (R)- or (S)-BTM catalyst. For β-galactosides with a free 2-O /3-O diol, we predict that (R)-BTM catalyst prefers to acylate 2-OH, while the (S)-BTM catalyst selectively acylates 3-OH.

For both α- and β-mannosides with a free 3-O/4-O diol, we expect selective acylation of 3-OH using (R)-BTM catalyst, because 3-OH is favored while 4-OH is disfavored under this situation. The prediction for L-rhamnosides using (R)-BTM should be the same as D-mannosides using (S)-BTM, and vice versa.

Since the establishment of the predictive model, collaborators from Tang's research group have studied the site-selective acylation using some of the representative carbohydrates as substrates.

Utilizing computational modeling we had identified that when reacting a protected α-O-glucoside with an aromatic protecting group with (R)-BTM, the 3-OH acylation "C-H down" TS was stabilized by a cation-π interaction. Since then, Tang's research group studied the effect this interacting aromatic group has on the site-selectivity.

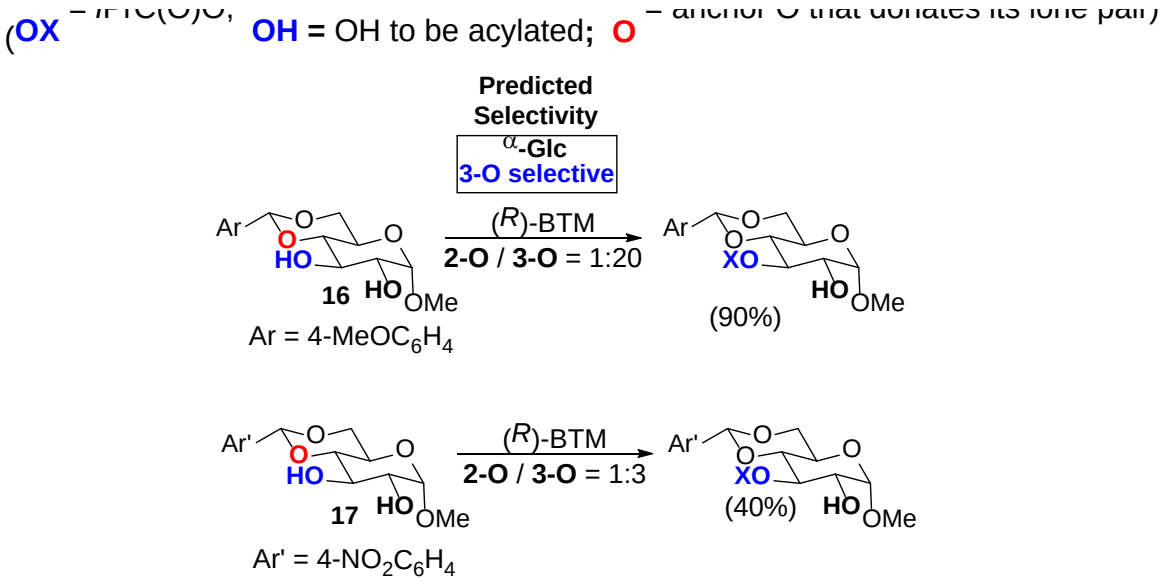

Figure 21 Effect of Aromatic Protecting Group on Site-selectivity of α-O-glucosides

From the experimentally determined selectivity, Tang's group observes that substrate **16** is more selective (2-O / 3-O = 1:<20) than **17** (2-O / 3-O = 1:3). Substrate **17** has an electron deficient

aromatic group (4-$NO_2C_6H_4$) which make a weaker cation-π. Because the 3-OH acylation "C-H down" TS is stabilized by a cation-π interaction, a weaker cation-π interaction will translate to a smaller $\Delta\Delta G^{\ddagger}$, which results in lower observed selectivity.

In another example, collaborators experimentally verified that β-galactosides substrates **18** and **19** reacted according to the predicted selectivity (2-O selective). By switching the substituent on the anchor oxygen from methyl group (**18**) to a more electron rich aromatic group (4-$MeOC_6H_4$ in **19**) a better selectivity was obtained. The more electron rich anchor oxygen in **19** forms a stronger cation-n interaction which stabilizes the favored TS.

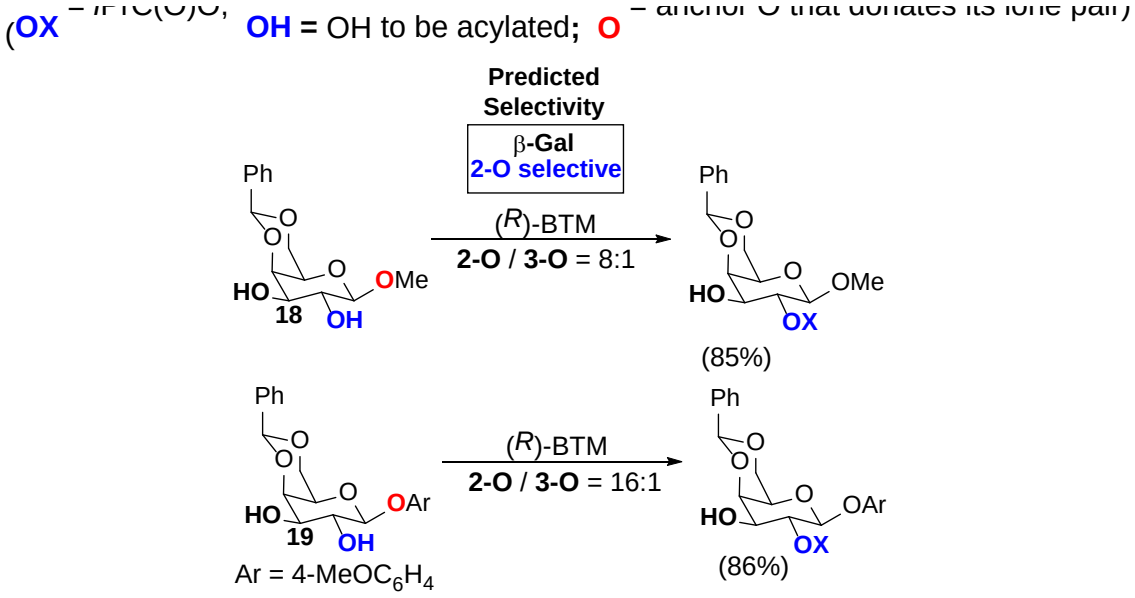

Figure 22 Effect of Anchor Oxygen Substitution on Site-selectivity of β-galactosides

Finally, Tang's group has also evaluated the site-selectivity of 3,4 diols for some example substrates. From our site-selectivity rules base on cation-n interactions, substrate **20** (β-mannoside) and **21** β-rhamboside are predicted to be 3-OH selective. Interestingly, the observed selectivity ratio favors the predicted 3-OH product.

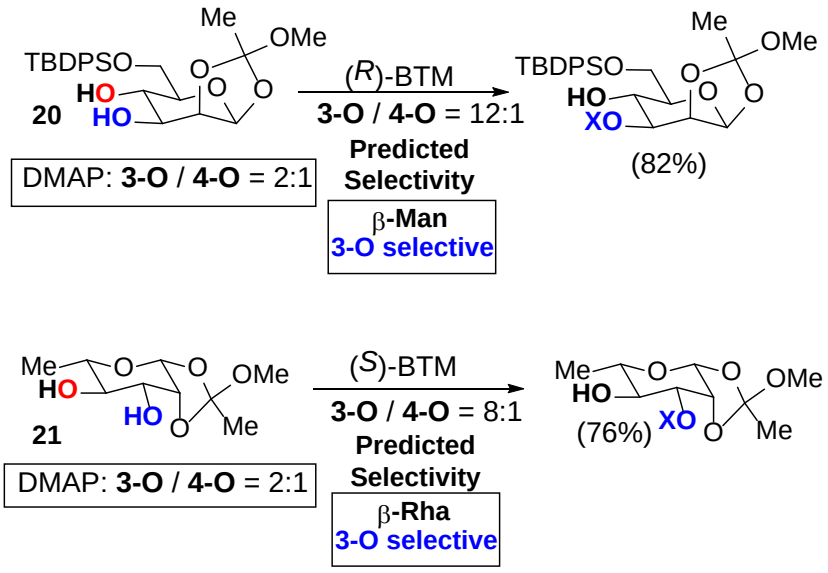

Figure 23 Site-selective acylation of trans-3,4-diols

2.11 BENCHMARK OF COMPUTATIONAL METHODS

From the experimentally reported product ratio we can estimate a $\Delta\Delta G^{\ddagger}_{exp}$ value to use as a standard and compare it to $\Delta\Delta G^{\ddagger}$ calculated by different computational methods. For an irreversible reaction where different products are unable to interconvert, the chemical kinetics of the system can be described using the Curtin–Hammett principle. This way we can estimate the difference in energy between two transition states from the experimentally observed product distribution ratio.

$$\Delta\Delta G^{\ddagger}_{exp} = -RT\ln(2\text{-}O/3\text{-}O)$$

$R = 0.001987$ kcal K^{-1} mol^{-1}.

$T = 295K$

To ensure that the conclusions obtained from the DFT calculations are not affected by the choice of computational methods, we calculated the activation energy differences of all five reactions using a few different computational methods. The methods tested include using M06L/6-31G(d) rather than M06-2X(d) for geometry optimizations, using a different solvation model (CPCM) for single point energy calculations, using the ω-B97xD functional instead of M06-2X for single point energies, using the harmonic oscillator approximation (the default method in Gaussian 09) for thermal corrections. The difference between using the "ultrafine" grid and the default integration grid in Gaussian 09 for geometry optimization was also tested. The computed relative activation free energies ($\Delta\Delta G^{\ddagger}$) are summarized in **(Tables 1-4)**.

Table 1 Computed site-selectivity of (*R*)-BTM-catalyzed acylation of *α*-*O*-glucoside **5a**

Entry	Method for Geometry Optimization	Method for Single Point Energy Calculation	Δ*G* Approximation	ΔΔ*G*‡ (kcal/mol) 2-O	3-O
1	M06L/6-31G(d)[a]	M06-2X/6-311++G(d,p)/Gas	Harmonic	3.4	0.0
2		M06-2X/6-311++G(d,p)/SMD		0.7	0.0
3		M06-2X/6-311++G(d,p)/CPCM		2.2	0.0
4		M06-2X/6-311++G(d,p)/Gas	Quasiharmonic	3.9	0.0
5		M06-2X/6-311++G(d,p)/SMD		1.7	0.0
6		M06-2X/6-311++G(d,p)/CPCM		2.7	0.0
7	M06L/6-31G(d)[b]	M06-2X/6-311++G(d,p)/SMD		1.3	0.0
8		ω-B97xD/6-311++G(d,p)/SMD		2.4	0.0
9	M06-2X/6-31G(d)[a]	M06-2X/6-311++G(d,p)/SMD	Harmonic	1.0	0.0
10			Quasiharmonic	2.1	0.0
11	M06-2X/6-31G(d)[b]		Harmonic	1.6	0.0
12			Quasiharmonic	2.2	0.0
			$\Delta\Delta G^{\ddagger}_{exp}$	1.8	0.0

[a] The default integration grid in Gaussian 09 was used. [b] The "ultrafine" integration grid in Gaussian 09 was used.

Table 2 Computed site-selectivity of (S)-BTM-catalyzed acylation of *α*-*O*-glucoside **5a**.

Entry	Method for Geometry Optimization	Method for Single Point Energy Calculation	Δ*G* Approximation	ΔΔ*G*‡ (kcal/mol) 2-O	3-O
1	M06L/6-31G(d)[a]	M06-2X/6-311++G(d,p)/Gas	Harmonic	0.0	0.6
2		M06-2X/6-311++G(d,p)/SMD		0.0	1.4
3		M06-2X/6-311++G(d,p)/CPCM		0.0	-0.4
4		M06-2X/6-311++G(d,p)/Gas	Quasiharmonic	0.0	0.3
5		M06-2X/6-311++G(d,p)/SMD		0.0	-0.7
6		M06-2X/6-311++G(d,p)/CPCM		0.0	-2.5
7	M06L/6-31G(d)[b]	M06-2X/6-311++G(d,p)/SMD		0.0	1.4
8		ω-B97xD/6-311++G(d,p)/SMD		0.0	0.2
9	M06-2X/6-31G(d)[a]	M06-2X/6-311++G(d,p)/SMD	Harmonic	0.0	1.1
10			Quasiharmonic	0.0	1.7
11	M06-2X/6-31G(d)[b]		Harmonic	0.0	3.6
12			Quasiharmonic	0.0	1.6
			$\Delta\Delta G^{\ddagger}_{exp}$	0.0	1.6

[a] The default integration grid in Gaussian 09 was used. [b] The "ultrafine" integration grid in Gaussian 09 was used.

Table 3 Computed site-selectivity of (*R*)-BTM-catalyzed acylation of *α*-*O*-glucoside **5b**

Entry	Method for Geometry Optimization	Method for Single Point Energy Calculation	Δ*G* Approximation	ΔΔ$G^{‡}$ (kcal/mol) 2-O	3-O
1	M06L/6-31G(d)[a]	M06-2X/6-311++G(d,p)/SMD	Harmonic	0.2	0.0
2			Quasiharmonic	-0.5	0.0
3	M06L/6-31G(d)[b]			-1.1	0.0
4	M06-2X/6-31G(d)[a]		Harmonic	3.9	0.0
5			Quasiharmonic	3.1	0.0
6	M06-2X/6-31G(d)[b]		Harmonic	3.6	0.0
7			Quasiharmonic	3.0	0.0
			$\Delta\Delta G^{‡}_{exp}$	1.1	0.0

[a] The default integration grid in Gaussian 09 was used. [b] The "ultrafine" integration grid in Gaussian 09 was used.

Table 4 Computed site-selectivity of (*S*)-BTM-catalyzed acylation of *α*-*O*-glucoside **5b**

Entry	Method for Geometry Optimization	Method for Single Point Energy Calculation	Δ*G* Approximation	ΔΔ$G^{‡}$ (kcal/mol) 2-O	3-O
1	M06L/6-31G(d)[a]	M06-2X/6-311+G(d,p)/SMD	Harmonic	0.0	3.0
2			Quasiharmonic	0.0	2.1
3	M06-2X/6-31G(d)[b]		Harmonic	0.0	3.5
4			Quasiharmonic	0.0	2.5
			$\Delta\Delta G^{‡}_{exp}$	0.0	1.8

[a] The default integration grid in Gaussian 09 was used. [b] The "ultrafine" integration grid in Gaussian 09 was used.

Generally, the computationally predicted site-selectivities are not affected by the choice of computational methods in most cases. The differences in the predicted 2-O/3-O selectivities in Table 1 and 2 indicate using the meta-hybrid-GGA functional M06-2X for geometry optimization provides much better agreement with experiment than using geometries optimized with the local functional M06L. On the other hand, the effects of integration grid and the difference between the quasiharmonic and harmonic approximations are both relatively small. Based on these benchmark

results, the M06-2X/6-311++G(d,p)/SMD//M06-2X/6-31G(d) level of theory using “ultrafine” grid and quasiharmonic approximation was chosen as the computational method for the present study.

2.12 CONCLUSIONS

Just based on the cation-n interaction alone, we can differentiate carbohydrate hydroxyl groups in a variety of different settings. The cation-n interaction proved to be a reliable tool for the prediction of site-selectivity. We expect that the above systematic strategy for differentiating hydroxyl groups will significantly simplify the synthesis of carbohydrate building blocks. Our computational investigations provide a thorough understanding of the underlying cation-n interaction for site-selectivity and a predictive model towards solving a long-standing challenging problem in chemistry.

Since oxygen lone pairs are prevalent in carbohydrates and many other complex natural products, the recognition of cation-n interaction as one of the determining factors for selectivity will have a profound effect on catalysis and other areas of chemistry beyond carbohydrate synthesis and glycobiology.

3.0 COMPUTATIONAL STUDIES ON THE CATALYTIC STEREOSELECTIVE SYNTHESIS OF A/ß ANOMERIC ESTERS.

3.1 CATALYTIC STEREOSELECTIVE SYNTHESIS OF A/ß ANOMERIC ESTERS

Tang's research group has developed catalytic stereoselective synthesis of α/ß anomeric esters. This reaction also makes use of chiral organocatalysts (R)-BTM, its enantiomer (S)-BTM and pivalic anhydride as the acylation reagent. [16]

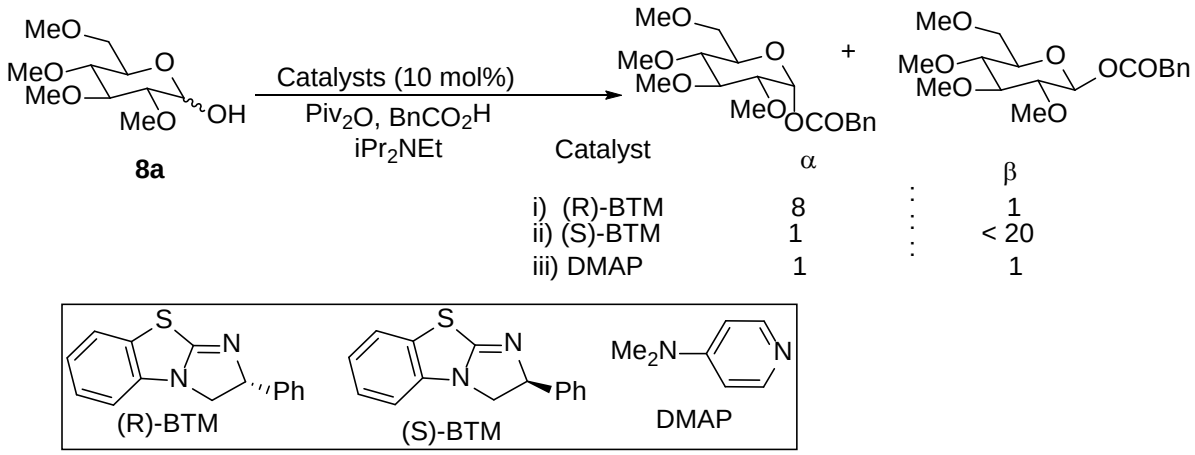

Figure 24 Catalytic Stereoselective Synthesis of α/β Anomeric Esters

The anomeric OH in glucoside **8a** is selectively acylated using (R)-BTM to afford an α/ß mixture with a ratio of 8:1 favoring the α stereochemistry. Using (S)-BTM will shift the α/ß mixture ratio to 1:<20 to favor the ß stereochemistry. In contrast, a 1:1 ratio of selectivity was observed using DMAP as the catalyst. The difference in the observed product ratio suggest that these reactions are under catalyst control. Like the previously discussed site-selective acylation, we hypothesize that

cation-n interactions between the positively charged acylated catalyst and a lone pair on an OR or OH group of the substrate are responsible for the observed selectivity.

Understanding these interactions may extend the scope of the site-selective acylation to many other carbohydrates and facilitate the development of new catalytic reactions.

3.2 CONFORMATIONAL ANALYSIS RESULTS FOR (S)-BTM-CATALYZED ACYLATION OF GLUCOSIDE 8A

To generate the acylation transition state conformers, we employed the same methodology discussed in the previous chapter. We identified the corresponding "C-H up" and "C-H down" TS conformers for both the α and β acylation.

Figure 25 summarizes the "C-H up", "C-H down" TS conformers for the acylation of **8a** with (S)-BTM**.** Experimentally this reaction favors β acylation with a ratio of <20:1. The computed free energy difference ($\Delta\Delta G^{\ddagger}$), which is shown for each TS conformer, indicates that conformer **10a-TS1** ($\Delta\Delta G^{\ddagger}$= 0.0 Kcal/mol) is the lowest energy TS conformer.

The α acylation "C-H down" conformer **9a-TS1** ($\Delta\Delta G^{\ddagger}$= 0.4 Kcal/mol) has the **2-OR** group above the BTM structure.

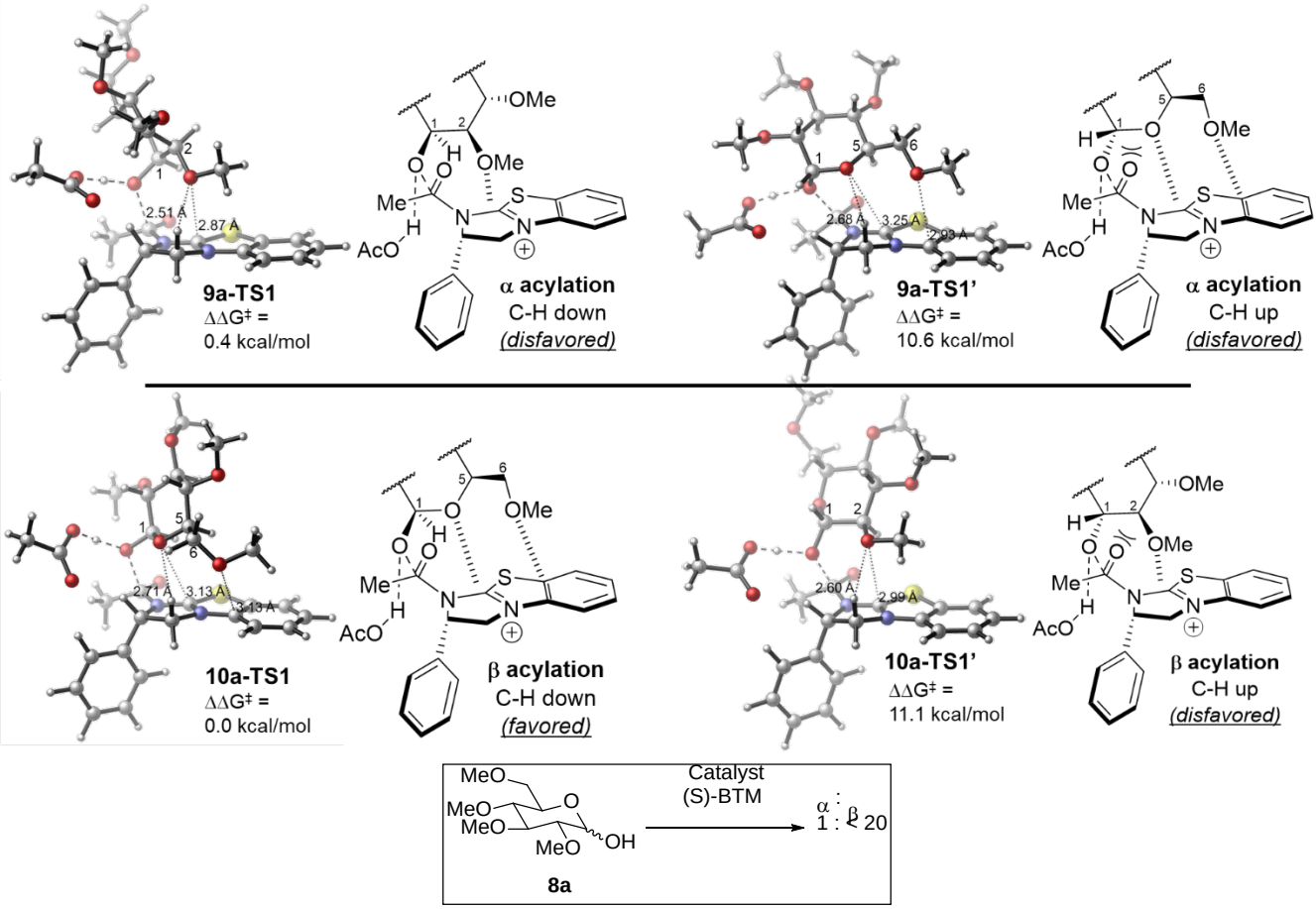

Figure 25 Transition state conformers of (*S*)-BTM-catalyzed synthesis of α/ß anomeric ester **8a**

The "C-H up" TS conformers for the **α** and **β** acylation were also computed (**9a-TS',10a-TS'**). The calculated free energy difference ($\Delta\Delta G^{\ddagger}$) for both was higher with an energy difference of $\Delta\Delta G^{\ddagger}$= 10.6 Kcal/mol $\Delta\Delta G^{\ddagger}$= 11.1 Kcal/mol, respectively, than the corresponding "C-H down" TS conformer, this matched the previous site-selectivity results in which the "C-H up" conformation is disfavored based on steric repulsions between the substrate and carbonyl O.

We suspect the pyranose O-1 anchor can form a stronger cation-n interaction because of its proximity to the acylated nitrogen in the BTM catalyst.

3.3 CONFORMATIONAL ANALYSIS RESULTS FOR (R)-BTM-CATALYZED ACYLATION OF GLUCOSIDE 8A

The "C-H up", "C-H down" TS conformers for the acylation of **8a** with (R)-BTM are summarized in **Figure 26**. This reaction has an experimental selectivity of 8:1 in favor the **α** product. The computed free energy difference ($\Delta\Delta G^{\ddagger}$), which is shown for each TS conformer, indicates that conformer **9a-TS2** ($\Delta\Delta G^{\ddagger}$= 0.0 Kcal/mol) is the computationally predicted product**,** which matches experimental selectivity.

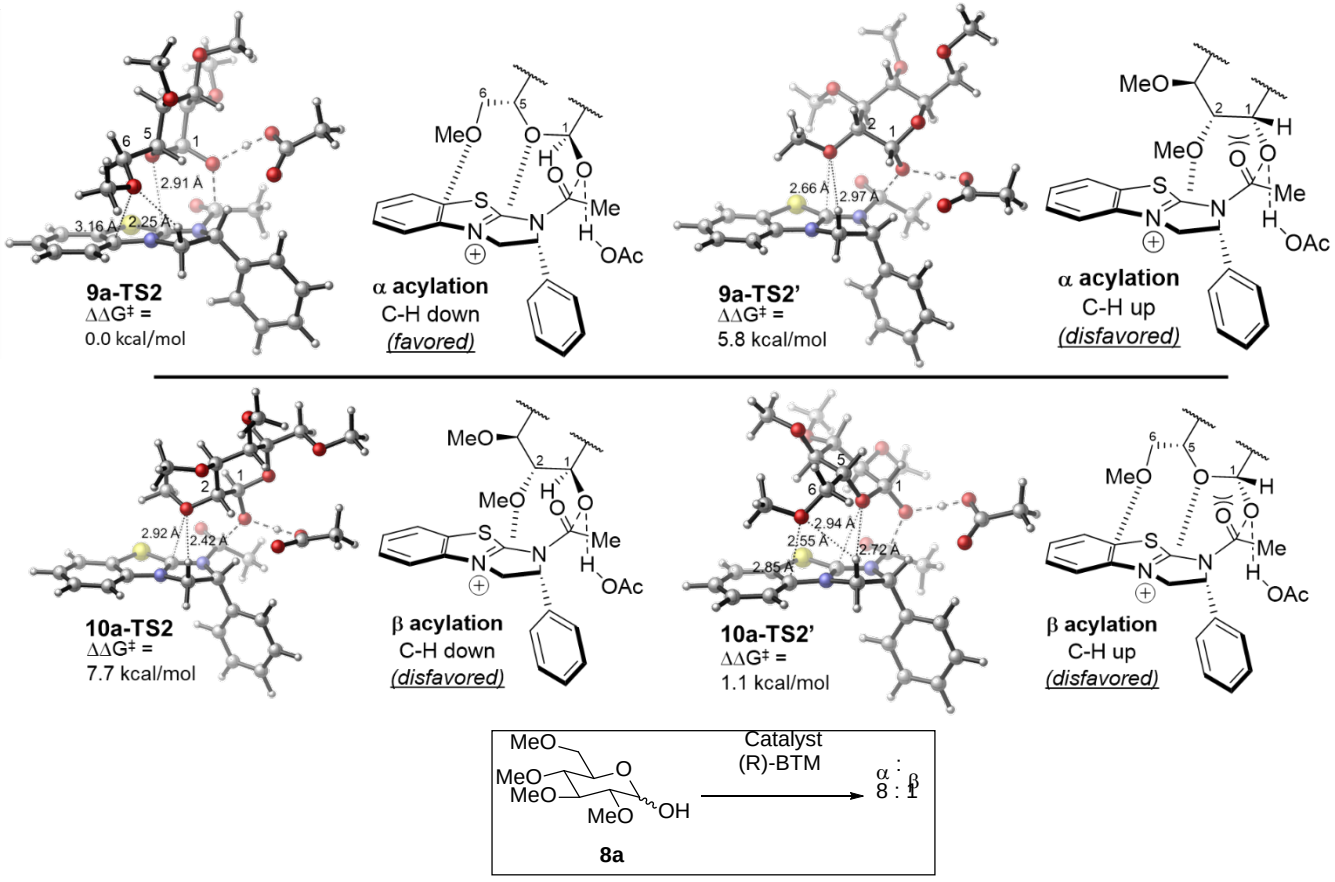

Figure 26 Transition state conformers of (*R*)-BTM-catalyzed synthesis of α/ß anomeric ester 8a**.**

For the case of (S)-BTM, the most stable TS conformer features a pyranose 1-O cation-*n* interaction. For (R)-BTM, the lowest energy conformer (**9a-TS2**) also has a pyranose 1-O and the 6-OR group above the catalyst.

The β acylation "C-H down" conformer **10a-TS2** ($\Delta\Delta G^{\ddagger}$= 7.7Kcal/mol) has the 2-OR group above the BTM structure.

The "C-H up" TS conformers for the α and β acylation were also computed (**9a-TS2',10a-TS2'**). The calculated free energy difference ($\Delta\Delta G^{\ddagger}$) for both was higher with an energy difference of $\Delta\Delta G^{\ddagger}$= 5.8 Kcal/mol $\Delta\Delta G^{\ddagger}$= 1.1 Kcal/mol, respectively, than the corresponding "C-H down" TS conformer.

The cation-n with the pyranose 1-O may be dictating the observed selectivity. As seen in the previous (S)-BTM catalyzed case, we hypothesize the pyranose O can form a more stable cation-*n* interaction because of its proximity to the acylated nitrogen in the BTM catalyst.

3.4 CONFORMATIONAL ANALYSIS RESULTS DISCUSSION

Like previously studied BTM catalyzed acylations, "C−H up" TS conformers are disfavored due to significant steric repulsions between the acylated catalyst and the adjacent carbons on the substrate. For both (R), (S)-BTM catalyst, most of the "C−H down" TS conformers are significantly more stable than the corresponding "C−H up" TS conformers.

The only exception is **10a-TS2'**, which is 6.6 kcal/mol lower than in energy than the corresponding "C−H down" conformer (**10a-TS2**). We suspect this is because the pyranose O-1 anchor can form a stronger cation-*n* interaction because of its proximity to the acylated nitrogen

in the BTM catalyst. This pyranose O-1 cation-n interaction is present in both favored TS conformers, **10a-TS1** and **10a-TS2**.

3.5 PREDICTIVE MODEL FOR IDENTIFYING FAVORABLE VS UNFAVORABLE SUBSTRATE-CATALYST CATION-N INTERACTIONS.

In the (S)-BTM-catalyzed reaction of 8a, this favorable cation-n interaction is augmented by having both the O in the pyranose ring and 6-OR interaction, that stabilizes the β-acylation TS (defined as "anchor" O in II) compared to the α-acylation TS, where the cation-n interaction is disfavored due having a weaker cation-n interaction with the 2-OMe group (defined as "disabled anchor" O in I)

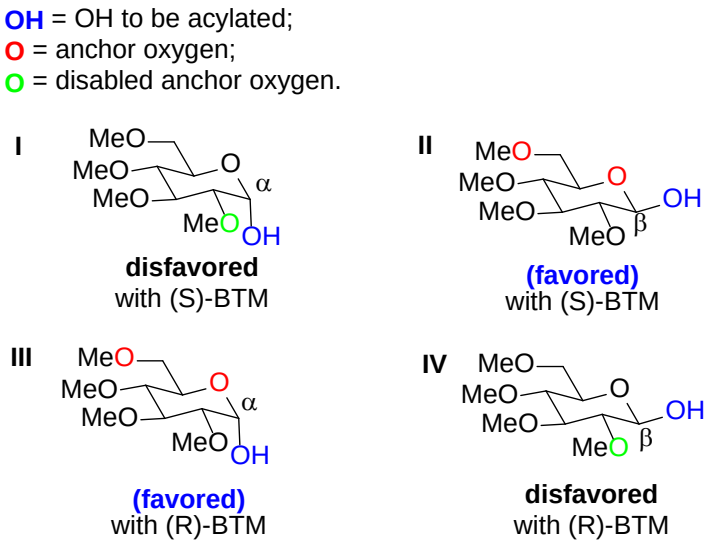

Figure 27 Working model for stereoselectivity based on cation-n Interactions

In the reaction with the (R)-BTM catalyst, the stereoselectivity is completely reversed to favor the α-acylation. The pyranose 1-O cation-n interaction is present in the favored TS (**9a-TS2**). The β-acylation TS (**10a-TS2**) is disfavored due having a weaker cation-n interaction with the 2-OMe group (defined as "disabled anchor" O in **IV**).

3.6 CONCLUSIONS

The computational analysis indicated the cation-n interaction is sensitive to the stereochemical environment around the O lone pair. The stereoselectivity of the acylation of anomeric OH is govern by a cation-n interaction with the pyranose 1-O which stabilizes the "C-H down" conformation. In this case of (S)-BTM this can happen in the α acylation TS and in the case of (R)-BTM this can happen in the β acylation TS.

BIBLIOGRAPHY

1. (a) Höfle, G.; Steglich, W.; Vorbrüggen, H. Angew. Chem. 1978, 90, 602; Angew. Chem., Int. Ed. Engl. 1978, 17, 569. (b) Spivey, A. C.; Arseniyadis, S. *Angew. Chem.* **2004**, 116, 5552; *Angew. Chem*., Int. Ed. Engl. **2004**, 43, 5436.

2. Kurahashi, T.; Mizutani, T.; Yoshida, J. I. *J. Chem. Soc. Perkin Trans.* I, 465e473

3. Larionov, E.; Mahesh, M.; Spivey, A.; Wei, Y.; Zipse, H. "Theoretical Prediction of Selectivity in Kinetic Resolution of Secondary Alcohols Catalyzed by Chiral DMAP Derivatives" *J. Am. Chem. Soc.* **2012**, 134, 9390-9399.

4. (a) Birman, V. B.; Uffman, E. W.; Jiang, H.; Li, X.; Kilbane, C. J. *J. Am. Chem. Soc.* **2004**, 126, 12226. (b) Birman, V. B.; Jiang, H. *Org. Lett.* **2005**, 7, 3445. (c) Birman, V. B.; Li, X.; Jiang, H.; Uffman, E. W. *Tetrahedron* **2006**, 62, 285. (d) Birman, V. B.; Li, X. *Org. Lett*. **2006**, 8, 1351. (e) Birman, V. B.; Guo, L. *Org. Lett*. **2006**, 8, 4859. (f) Birman,V. B.; Jiang, H.; Li, X. *Org. Lett*. **2007**, 9, 3237. (g) Birman, V. B.; Li, X. *Org. Lett*. **2008**, 10, 1115. (h) Li, X.; Liu, P.; Houk, K. N.; Birman, V. B. *J. Am. Chem. Soc*. **2008**, 130, 13836. (i) Li, X.; Jiang, H.; Uffman, E. W.; Guo, L.; Zhang, Y.; Yang, X.; Birman, V. B. *J. Org. Chem*. **2012**, 77, 1722

5. Shiina, I.; Nakata, K.; Ono, K.; Sugimoto, M.; Sekiguchi, A. "Kinetic Resolution of the Racemic 2-Hydroxyalkanoates Using the Enantioselective Mixed-Anhydride Method with Pivalic Anhydride and a Chiral Acyl-Transfer Catalyst" *Chem. Eur. J*. **2010**, 16, 167.

6. a) Wang, H.-Y.; Yang, K.; Yin, D.; Liu, C.; Glazier, D. A.; Tang, W. *Org. Lett*. **2015**, 17, 5272-5275; b) Wang, H.-Y.; Simmons, C. J.; Zhang, Y.; Smits, A. M.; Balzer, P. G.; Wang, S.; Tang, W. *Org. Lett*. **2017**, 19, 508-511.

7. Cintron-Rosado, G.; Xiao, G.; Glazier, D.; Xi, B.; Liu, C.; Liu, P.; Tang, W.; *J. Am. Chem. Soc*. **2017**, 139, 4346-4349

8. Frisch, M. J., Trucks, G. W., Schlegel, H. B., Scuseria, G. E., Robb, M. A., Cheeseman, J. R., Scalmani, G., Barone, V., Mennucci, B., Petersson, G. A., Nakatsuji, H., Caricato, M., Li, X., Hratchian, H. P., Izmaylov, A. F., Bloino, J., Zheng, G., Sonnenberg, J. L., Hada, M., Ehara, M., Toyota, K., Fukuda, R., Hasegawa, J., Ishida, M., Nakajima, T., Honda, Y., Kitao, O., Nakai, H., Vreven, T., Montgomery, J. A. Jr., Peralta, J. E., Ogliaro, F., Bearpark, M., Heyd, J. J., Brothers, E., Kudin, K. N., Staroverov, V. N., Kobayashi, R., Normand, J., Raghavachari, K., Rendell, A., Burant, J. C., Iyengar, S. S., Tomasi, J., Cossi, M., Rega, N., Millam, N. J., Klene, M., Knox, J. E., Cross, J. B., Bakken, V., Adamo, C., Jaramillo, J.,

Gomperts, R., Stratmann, R. E., Yazyev, O., Austin, A. J., Cammi, R., Pomelli, C., Ochterski, J. W., Martin, R. L., Morokuma, K., Zakrzewski, V. G., Voth, G. A., Salvador, P., Dannenberg, J. J., Dapprich, S., Daniels, A. D., Farkas, Ö., Foresman, J. B., Ortiz, J. V., Cioslowski, J., Fox, D. J. Gaussian 09, Revision D.01; Gaussian, Inc.:

9. Grimme, S., Antony, J., Ehrlich, S., Krieg, H. J. *Chem. Phys*. **2010**,132, 154104

10. Grimme, S. J. *Comput. Chem*. **2006**, 27, 1787

11. Marenich, A. V., Cramer, C. J., Truhlar, D. G. J. *Phys. Chem*. B, **2009**,113, 6378.

12. Ribeiro, R. F.; Marenich, A. V.; Cramer, C. J.; Truhlar, D. G. J. *Phys. Chem*. B, **2011**, 115, 14556.

13. a) Wheeler, S. E.; Bloom, J. W. G. J. *Phys. Chem*. A **2014**, 118, 6133; b) Wheeler, S. E.; Houk, K. N. J. *Phys. Chem*. A **2010**, 114, 8658; c) Pavlakos, I.; Arif, T.; Aliev, A. E.; Motherwell, W. B.; Tizzard, G. J.; Coles, S. J. Angew. *Chem. Int. Ed*. **2015**, 54, 8169.

14. Li, X.; Liu, P.; Houk, K. N.; Birman, V. B. "Origin of Enantioselectivity in Cf(3)-Pip-Catalyzed Kinetic Resolution of Secondary Benzylic Alcohols." *J. Am. Chem. Soc*. **2008** 130, 13836-13837).

15. Liu, P.; Yang, X.; Birman, V. B.; Houk, K. N. "Origin of Enantioselectivity in Benzotetramisole-Catalyzed Dynamic Kinetic Resolution of Azlactones." *Org. Lett*.,**2012**, 14, 3288-3291

16. a) Wang, H.-Y.; Yang, K.; Yin, D.; Liu, C.; Glazier, D. A.; Tang, W. *Org. Lett*. **2015**, 17, 5272-5275; b) Wang, H.-Y.; Simmons, C. J.; Zhang, Y.; Smits, A. M.; Balzer, P.; Wang, G. S.; Tang, W. *Org. Lett*. **2017**, 19, 508-511